IL-6 induced cGGNBP2 encodes a protein to promote cell growth and metastasis in intrahepatic cholangiocarcinoma

Hui Li[1,2,3,*], Tian Lan[1,2,*], Hailing Liu[1,2,*], Chang Liu[1], Junlong Dai[1], Lin Xu[2], Yunshi Cai[1,2], Guimin Hou[1,2], Kunlin Xie[1,2], Mingheng Liao[1,2], Jiaxin Li[1,2], Jiwei Huang[1,2], Kefei Yuan[1,2], Genshu Wang[4], Yong Zeng[1,2], Hong Wu[1,2]

[1]Department of Liver Surgery, Liver Transplantation Division, West China Hospital, Sichuan University, Chengdu, 610041, China.

[2]Laboratory of Liver Surgery, West China Hospital, Sichuan University, Chengdu, 610041, China.

[3]Department of Hepatobiliary Pancreatic Tumor Center, Chongqing University Cancer Hospital, Chongqing, 400030, China.

[4]Department of Hepatic Surgery and Liver Transplantation Center, the Third Affiliated Hospital of Sun Yat-sen University, Guangzhou, 510006, China.

*These authors contributed equally to this work.

Correspondence

Hong Wu, Yong Zeng, Kefei Yuan, Department of Liver Surgery, Liver Transplantation Division, Laboratory of Liver Surgery, West China Hospital, Sichuan University, No. 37 of Guoxue Lane, Wuhou District, Chengdu, 610041, China. Tel: +86-028-85422871. Fax: +86-028-85422871. E-mails: wuhong@scu.edu.cn (Hong Wu); zeng_y@scu.edu.cn (Yong Zeng); ykf13@163.com (Kefei Yuan).

Genshu Wang, Department of Hepatic Surgery and Liver Transplantation Center, the Third Affiliated Hospital of Sun Yat-sen University, No.600 of Tianhe Road, Guangzhou, 510006, China. Tel: +86-020-85252177. Fax: +86-020-85252276.

wgsh168@163.com.

Table of contents

Methods

Patient cohorts and tissues

Tumor tissues were obtained from surgical specimen archives of 136 ICC patients without any preoperative treatments at West China Hospital (Sichuan University, Chengdu, China) from 2009 to 2018. Frozen tissues were used for quantitative reverse transcription PCR (qRT-PCR) and western blotting analyses, while formalin-fixed and paraffin-embedded (FFPE) tissues were used for immunohistochemistry analyses. Of them, 40 patients were tested for preoperative serum IL-6, IL-8, IL-10 and TNF-α levels. 20 patients with hepatic hemangioma were also measured serum IL-6 and collected for normal hepatic tissues.

ICC cells, non-cancerous cholangiocytes and CAFs were freshly isolated from 20 ICC patients. Human tissues and relative clinical data collection were conformed to the ethical guidelines of the 1975 Declaration of Helsinki and approved by the Ethics Committee of West China Hospital. Signed informed consents were obtained from patients or their direct relatives.

RNA-seq

Total RNAs were extracted using Trizol Reagent (Invitrogen, CA, USA). The high-throughput sequencing and analyses for circRNAs were carried out by Novogene Technology Co., LTD (Beijing, China). The clustering of the index-coded samples was performed on a cBot Cluster Generation System using TruSeq PE Cluster Kit v3-cBot-HS (Illumia) according to the manufacturer's instructions. After cluster generation, the libraries were sequenced on an Illumina Hiseq 4000 platform. The circRNAs were detected and identified using find_circ[1]. Total RNAs of indicated cells were used for mRNA sequencing on an Illumina Novaseq™ 6000 platform at the LC-BIO Bio-tech ltd (Hangzhou, China). Gene set enrichment analysis (GSEA) was applied for pathway analysis.

Cell lines and reagents

The cell lines were purchased from the Cell Bank of Academy of Science (Shanghai, China) and cultivated in recommended medium, supplemented with 10% fetal bovine serum (FBS), 100 U/mL penicillin and 100 μg/mL streptomycin. Short tandem repeat (STR) profiling was used to identify that the cells used in this work were not contaminated by other cells. The recombinant Human IL-6 was purchased from PeproTech (Rocky Hill, NJ, USA) and used in 50 ng/ml unless indicated. Time for treatment was 24 hours unless indicated. To inhibit the phosphorylation of STAT3, 20 μM C188-9 (S8605, Selleck, Houston, TX, USA) or 20 μM BP-1-102 (S7709, Selleck) were added to the culture medium for 24 hours.

Western blotting (WB)

Total proteins were extracted from cells or tissues which were lysed in RIPA buffer containing protease and phosphatase inhibitor (Thermo Fisher Scientific, CA, USA) and quantified using BCA protein assay kit (Thermo Fisher Scientific). Proteins were separated by SDS-PAGE and transferred to nitrocellulose membrane. Then the membranes were blocked with 5% BSA and incubated with indicated primary antibodies overnight at 4°C, followed by horseradish peroxidase-conjugated secondary antibodies. The immunoreactivity was visualized using ECL reagents (Beyotime Biotechnology, China). The densitometry analysis was performed using Image J (National Institutes of Health, Bethesda, MD, USA). The primary antibodies were listed in Table S6.

RNA isolation and quantitative real-time PCR

Total RNA of cells and tumor tissues were extracted using Total RNA Isolation Kit (Foregene, Chengdu, China) according to the manufacturer's instructions. The first-strand cDNA was synthesized using HiScript II Reverse Transcriptase Kit (Vazyme Biotech, Nanjing, China). Quantitative real-time PCR was performed using ChamQTM

SYBR@ qPCR Master Mix (Vazyme). All the real-time PCR reactions were performed in triplicate on CFX96TM Touch Real-Time PCR System (Bio-Rad, California, USA) and the relative RNA expression was quantitated using the comparative $2^{-\Delta\Delta CT}$ method. Patients were divided into two groups according to the relative expression using X-tile software. β-actin or U6 was utilized as endogenous control. The primer sequences were summarized in Table S7.

Vector and transfection

Overexpression of cGGNBP2 was performed as previously described[2, 3]. In brief, the genomic region for cGNNBP2 with its flanking reverse complementary sequences from intron 2 to intron 6 [a 1915-nt region of the GGNBP2 gene, spanning from forward reverse complementary match (RCM) of intron 2 to reverse RCM of intron 6] was amplified from RBE genomic DNAs. Wild type pLCDH plasmid was cloned by inserting the 1915-nt region of the GGNBP2 gene. DNA sequences with FRCM (reverse complementary sequences in intron 2) or (and) RRCM (reverse complementary sequences in intron 6) depletion were synthesized by PEPTBIO (PEPTBIO, Wuhan, China) and cloned into pEZ-Lv201 vector as mentioned above. The linear cGGNBP2-184aa-HA (predicted ORF of cGGNBP2 with DNA sequences of HA) and IRES-MUT (a 1915-nt region containing mutant IRES) plasmids were also constructed as mentioned above. Plasmids used for luciferase reporter assays were constructed by VectorBuilder (Guangzhou, China). The sequences of potential IRES, truncation mutant or IRES with point mutation were amplified and inserted between renilla luciferase (Rluc) and the firefly luciferase (FLuc).

The transient transfection of small interfering RNAs was performed using Genmute™ Reagent (SignaGen Laboratories, Maryland, USA) following the manufacturer's protocol. The plasmids were transfected using GenJet™ Plus reagent (SignaGen Laboratories, Maryland, USA).

Construction of stable cell lines

The same cDNA oligonucleotides with cGGNBP2 siRNA (the sequences were shown in Table S8) were synthesized with annealing, double-strand oligonucleotides were inserted into shRNA expression plasmid pWSLV-sh08 (GeneCopoeia, CA, USA). All plasmids were transfected into HEK293T cells for lentivirus production[4]. To generate stable cell lines, the cell lines were lentivirus infected, followed by puromycin selection.

Fluorescent In Situ Hybridization (FISH)

Cells were washed with PBS and fixed in 4% paraformaldehyde at room temperature for 20 minutes. Then the cells were permeabilized using PBS containing 0.2% Triton X-100 on ice for 10 minutes. FISH was performed using Fluorescent In Situ Hybridization Kit (RiboBio, Guangzhou, China), in accordance with manufacturer's instructions. The anti-cGGNBP2 oligodeoxynucleotide probe (Table S3), which was conjugated with Cy3 was synthesized by Sangon Biotech. Cy3-labeled anti-18S or U6 oligodeoxynucleotide probes (RiboBio) were used as controls. Then cells were hybridized in hybridization solution for 16 hours at 50℃ in a moist chamber. After that, cells were washed for 30 min in 25% deionized formamide/2×SSC at 50°C and then 30 min in 2×SSC at 42°C. For microscopy, the cells on the coverslips were stained with DAPI and scanned using an A1R+MP confocal laser microscope (Nikon, Tokyo, Japan).

Immunofluorescence (IF)

Cells were briefly rinsed using PBS and fixed in 4% paraformaldehyde at room temperature for 20 minutes. Then the cells were permeabilized with PBS containing 0.2% Triton X-100 on ice for 10 minutes and blocked with 5% BSA at room temperature for 1 hour. Primary antibodies were incubated overnight at 4°C and washed three times. Secondary antibodies were incubated for 1 hour at 37°C in lucifugal chamber. Immunostaining was conducted using appropriate primary and secondary antibodies.

The primary antibodies used for IF analysis were summarized in Table S6. After counterstained with DAPI, images were acquired using AX10 imager A2 microscope (Carl Zeiss MicroImaging).

Tissue microarray and immunohistochemistry (IHC)

A tissue microarray was constructed as previously described. IHC assay was performed on the microarray as we described before[5]. Microarrays were deparaffinized in xylene and rehydrated in graded ethanol. Subsequently, the microarrays were subjected to antigen retrieval using Tris-EDTA buffer (pH 9.0) for 30 minutes at room temperature. Next, microarrays were treated with 0.3% H_2O_2 for 10 minutes at room temperature to inhibit endogenous peroxidase activity, blocked with 5% BSA for 1 hour. Primary antibodies were incubated overnight at 4°C and washed three times. Secondary antibodies were incubated for 1 hour at 37°C. The immunohistochemical staining was evaluated by the histochemistry score by two separate pathologists who were blinded to patient characteristics. The primary antibodies for IHC assays were shown in Table S6.

Evaluation of tumor infiltrating lymphocytes (TILs)

Microarrays were deparaffinized and rehydrated, followed by incubation with eosin and hematoxylin. The tumor infiltrating lymphocytes were assessed based on HE staining according to a previous study[6]. TILs were evaluated in the tumor cell compartment under light microscopy (×200 magnification, ×20 objective lens, and ×10 ocular lens; 0.950 mm^2 per field).

Isolation of ICC cells, non-cancerous cholangiocytes and cancer-associated fibroblasts (CAFs)

ICC tumor tissues or normal hepatic tissues were cut into small pieces and dissociated using 0.75 μg/μL collagenase I (Sigma-Aldrich, St. Louis, MO, USA) and 0.1% trypsin (Gibco, CA, USA) at 37°C for 1 hour. Then the homogenate was collected and

successively filtered through a 70 μm and 40 μm cell strainer. Next, the dissociated cells were re-suspended. CAFs were purified using magnetic activated cell sorting after incubation with anti-fibroblast microbeads (Miltenyi Biotec, Auburn, CA, USA) for 30 minutes. The positive cells were collected after passing through a MiniMACS separator[7]. The dissociated cells were stained by a fluorescent antibody positive selection biliary marker EpCAM (Biolegend, 1:100) and negatively selected for by CD45 (BD Biosciences, 1:100) and CD11b (BD Biosciences, 1:100) for 30 minutes at 4°C. After washing, cholangiocytes were sorted by FACS utilizing a BD FACSAria II, using the 100μm nozzle[8].

Northern blotting (NB)

RNA was extracted using Trizol reagent (Invitrogen, CA, USA). The NB assay was performed using a Northern blot Kit (Thermo Fisher Scientific) according to the manufacturer's instructions. In brief, a total of 30 μg RNA was treated with RNase R and denatured in formaldehyde, followed by electrophoresing in a 1% agarose–formaldehyde gel. Then the RNA was transferred onto a Hybond-N+nylon membrane (GE Healthcare, USA) and subsequently hybridized with a digoxigenin-labelled cGGNBP2 DNA probe. Thereafter, a DIG Oligonucleotide 3'-End Labeling Kit (Roche Diagnostics, IN, USA) was used applied for the development of the bound RNA. The intensity of signals was scanned by X-ray films with chemiluminescence substrate CSPD (Roche Diagnostics). GAPDH was used as a control. The DNA probe was listed in Table S8.

In vitro cell proliferation assays and cell cycle assay

For Cell Counting Kit-8 (CCK-8) assay, a total of 2000 cells were suspended using 100 μl medium and added into triplicate wells of 96-well plate. 10 μl CCK-8 (Beyotime Biotechnology, Shanghai, China) was added to each plate and subsequently incubated at 37 ℃ for 2 hours. The absorbance was measured at 450 nm using the EonTM

Microplate Reader (BioTek, VT, USA) at the indicated time. For colony formation assay, the indicated cells were seeded into triplicate wells of a 6-well plate at a density of 1000 cells/plate and cultured for 14 days. The colonies were fixed with 4% paraformaldehyde and stained using 0.1% crystal violet. The plates were scanned and analyzed using Celigo Image Cytometer (Nexcelom Bioscience, MA, USA). The EdU assay was performed using a Cell-Light EdU Apollo567 In Vitro Kit (RiboBio, Guangzhou, China) in accordance with its protocol. The proliferation rate was calculated by EdU positive rate. Cell cycle of indicated cells was examined using a Cell Cycle Kit (4A Biotech, Beijing, China) according to the manufacturer's protocols and analyzed by the CytoFLEX Research Flow Cytometer (Beckman Coulter, CA, USA).

In vitro migration assays and invasion assay

For the wound-healing assay, indicated cells were seeded in triplicate into 6-well plates. A 10-μl plastic pipette tip was applied to the scratch wound when the monolayers of cells reached at a density of 95%. The cells were rinsed using PBS to remove any floating cells and subsequently cultured in an FBS-free medium. The wound closure was monitored by a microscope and analyzed using Image J (National Institutes of Health, Bethesda, MD, USA) at the indicated time. For migration and matrigel invasion assays, Transwell chambers (8.0 μm pore size, Corning Costar, Kennebunk, USA) were used according to the manufacturer's protocols. For migration assay, 3×10^4 cells were suspended in an FBS-free medium and then seeded into the upper chamber. For matrigel invasion assay, 5×10^4 cells were suspended in an FBS-free medium and seeded into the upper chamber that pre-coated with matrigel. The medium containing 10% FBS were added into the lower chamber. After incubation for 24 or 48 hours at 37 ℃, cells that migrated or invaded onto the lower surface of lower chambers were fixed and stained. 5 random microscopic fields were counted for each group using Image J.

In vivo xenograft assays

The in vivo animal experiments were approved by the Animal Ethics Committees of West China Hospital (Sichuan University, Chengdu, China) and performed as we previously described[9]. 5-week-old male BALB/c nude mice were purchased from Vital River Laboratories (Beijing, China) and used for in vivo xenograft assays. For subcutaneous xenograft model, 2×10^6 stable transfected cells were suspended in 100 μl serum-free medium and injected subcutaneously into the right axilla of mice. Tumor volumes were measured weekly and calculated by using the formula of $0.52 \times \text{length} \times \text{width}^2$. The weight of subcutaneous xenograft was measured after the mice were sacrificed. BP-1-102 was administered through oral gavage (3 mg/kg body weight) every day after establishment of in vivo models until sacrifice. Recombinant human IL-6 (2 mg/kg body weight) was intraperitoneally injected three times a week. IL-6 neutralizing antibody (10 mg/kg body weight) was intraperitoneally injected prior to administrating IL-6. For liver orthotopic-implanted models, 1×10^6 cells were transplanted into the left lobes of the liver. Mice were sacrificed 4 weeks after implantation and then the livers were scanned by the IVIS@ Lumina II system (Caliper Life Sciences, Hopkinton, MA, USA). For lung metastasis models, 2×10^6 cells were injected through tail veins. After 6 weeks, the mice were visualized using the IVIS@ Lumina II system 15 min after intraperitoneal injection of 3.0 mg of D-Luciferin (ABP Biosicences, USA) in 200 μl of PBS without calcium or magnesium. Subsequently, the mice were sacrificed, and the lungs were visualized by the IVIS@ Lumina II system. The livers and lungs embedded in paraffin and the metastases were confirmed by hematoxylin and eosin staining. The animal experiments were strictly implemented in compliance with the National Institutes of Health Guidance for the Care and Use of Laboratory Animals.

Actinomycin D assay

RBE cells were seeded into 5 wells of a 6-well plate at a density of 2×10^5 cells/well. Cells were treated with actinomycin D (1 μg/ml) and harvested after 0, 4, 8, 12 and 24 hours, respectively. The relative RNA expression levels of cGGNBP2 and mGGNBP2 were analyzed by real-time PCR, and normalized by the values of 0-hour group.

RNase R treatment

Total RNA was extracted from RBE cells using Trizol reagent (Invitrogen). Approximately 3 μg RNA was subjected to RNase R treatment (Epicentre, 10 U, 37 °C, 30 min), followed by incubation at 75 °C for 10min to deactivate the RNase R. Circ7, an already known circRNA, was used for control. The relative RNA expression levels of cGGNBP2 and mGGNBP2 were analyzed by real-time PCR and normalized to the values of the mock group (without RNase R treatment).

Immunoprecipitation (IP) and mass spectrometry (MS)

The IP assay was performed using Pierce Crosslink Magnetic IP/Co-IP Kit (Thermo Fisher Scientific) according to the manufacturer's instructions. Briefly, cells were lysed in RIPA buffer and incubated with protein A/G magnetic beads that bind to primary antibodies previously. Then, the antibody-crosslinked beads were rinsed using PBS and eluted in the elution buffer. The immune complexes were separated via SDS-PAGE and analyzed by immunoblotting. For MS analysis, the gels were stained with Coomassie brilliant blue (Beyotime Biotechnology, China). The gel bands of interest were manually cut into small particles, followed by acetonitrile dehydration and trypsin digestion. After that, the digested peptides were analyzed by a Q-Exactive mass spectrometer (Thermo Fisher Scientific) equipped with a Nanospray Flex source (Thermo Fisher Scientific). The MaxQuant was used to search all of the raw data thoroughly against the protein database (UniProt)[10].

Subcellular RNA fractionation

Cytoplasmic and nuclear RNA fractions were extracted with the PARIS™ Kit (Thermo Fisher Scientific, CA, USA), according to its instructions, and subsequently analyzed by real-time PCR. β-actin mRNA was used as the endogenous cytoplasmic control. U3 small nuclear RNA was used as the endogenous nuclear control.

Subcellular protein fractionation

Nuclear and cytoplasmic protein fractions were extracted with the NE-PER™ Nuclear and Cytoplasmic Extraction Reagents (Thermo Fisher Scientific, CA, USA) according to its protocols. The extracted protein samples were subsequently separated on SDS-PAGE gels and analyzed by WB assays. GAPDH was used as the endogenous cytoplasmic control and Histone H3 was used as endogenous nuclear control.

Luciferase reporter assays

The plasmids, of which the renilla luciferase (Rluc) was placed in front and the firefly luciferase (Luc) was placed in the back, were constructed by VectorBuilder (Guangzhou, China). The potential IRES sequences of cGGMNP2 and mutant were amplified and inserted in the middle of Rluc and Luc. The plasmids were transfected according to the manufacturer's instructions of Lipofectamine 3000 (Invitrogen, Carlsbad, CA, USA). After culture for 48 hours, the luciferase activity was evaluated using the Duo-Luciferase HS Assay Kit (GeneCopoeia, CA, USA) in accordance with the manufacturer's instructions. The relative results were shown as Luc/Rluc activity.

Cross-Linked RNA immunoprecipitation assays

Indicated cells were treated with 0.3% formaldehyde to cross-link and then quenched by glycine solution. Cross-Linked RNA immunoprecipitation assays were conducted according to the manufacturer's protocols of Magna RIP™ RNA-binding Protein Immunoprecipitation Kit (Millipore, Massachusetts, USA). Briefly, cell lysates were incubated with magnetic beads that bind to an antibody against DHX9 (Abcam, Cambridge, USA) or normal IgG (Millipore, Massachusetts, USA) previously. After

incubation overnight at 4 °C, the magnetic beads were rinsed and then digested using proteinase K buffer for 45 min at 55 °C. The enriched RNAs were extracted using phenol: chloroform: isoamyl alcohol (125:24:1), followed by purification. Subsequently, the immunoprecipitated RNAs were analyzed by real-time PCR to evaluate the enrichment of target RNAs to the target proteins.

Statistical analysis

All experiments were performed at least three times unless otherwise noted. Data were exhibited as mean ± standard deviation (SD). Comparisons were performed using student's t-test, one-way ANOVA, or Mann-Whitney U-test, as appropriate. Correlation between two groups was measured by the Pearson correlation analysis. The optimal cutoff values of serum IL-6 level and the relative cGGNBP2 expression in ICC tissue were determined using X-title software. Survival curves were plotted using the Kaplan-Meier method and tested by log-rank test. Cox proportional hazards regression model was utilized to evaluate the potential independent prognostic factors. A two-tailed P value < 0.05 was considered statistically significant. All statistical analyses were carried out by applying SPSS (version 23.0, SPSS Inc., Chicago, IL, USA), GraphPad Prism (version 8.0, La Jolla, CA, USA) or MedCalc software (version 15.2.2).

Supplementary figures

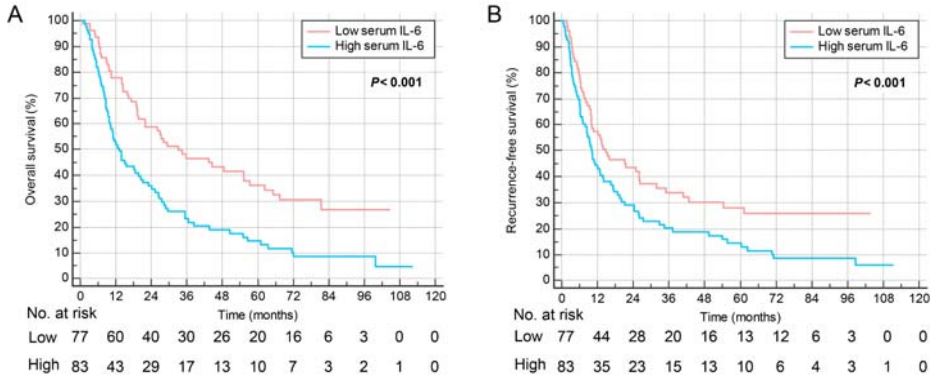

Fig. S1. Increased serum IL-6 level associates with poor prognosis of ICC patients. Kaplan-Meier survival analysis showing the correlation between serum IL-6 expression and OS (A) or RFS (B). The cut-off value of serum IL-6 was determined by X-tile. OS, overall survival; RFS, recurrence-free survival.

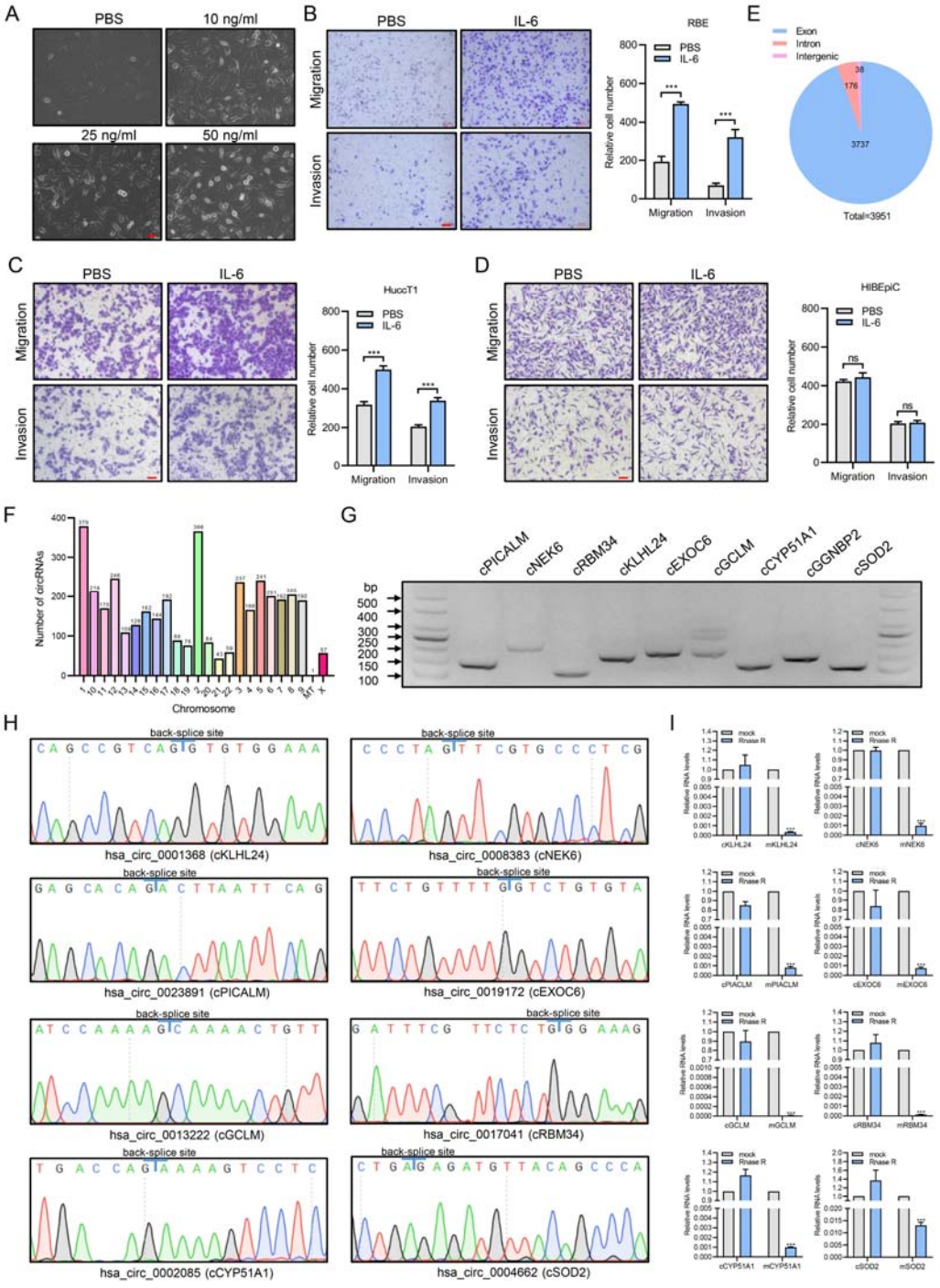

Fig. S2. IL-6 promotes migration and invasion of RBE cells. (A) Phase-contrast micrographs of RBE cells treated with IL-6 for the indicated time. Scale bar, 100 μm. **(B) and (C)** The migration and invasion of RBE or HuccT1 cells treated with IL-6 or PBS. IL-6, 50 ng/ml for 24 hours. Scale bar, 100 μm. **(D)** The migration and invasion

of normal cholangiocytes (HIBEpiC) treated with IL-6 or PBS. IL-6, 50 ng/ml for 24 hours. Scale bar, 100 μm. **(E)** Genomic origin of the annotated circRNAs identified by RNA-seq. **(F)** Chromosomal distributions of the annotated circRNAs. **(G)** qRT-PCR assays with divergent primers indicating the detection of nine circRNAs in RBE cells. **(H)** Sanger sequencing validated the back-splice sites of the candidate circRNAs. **(I)** qRT-PCR analyses for the relative expression of candidate circRNAs and the relative mRNAs after treatment with RNase R in RBE cells. ***, $P < 0.001$; ns, not significant.

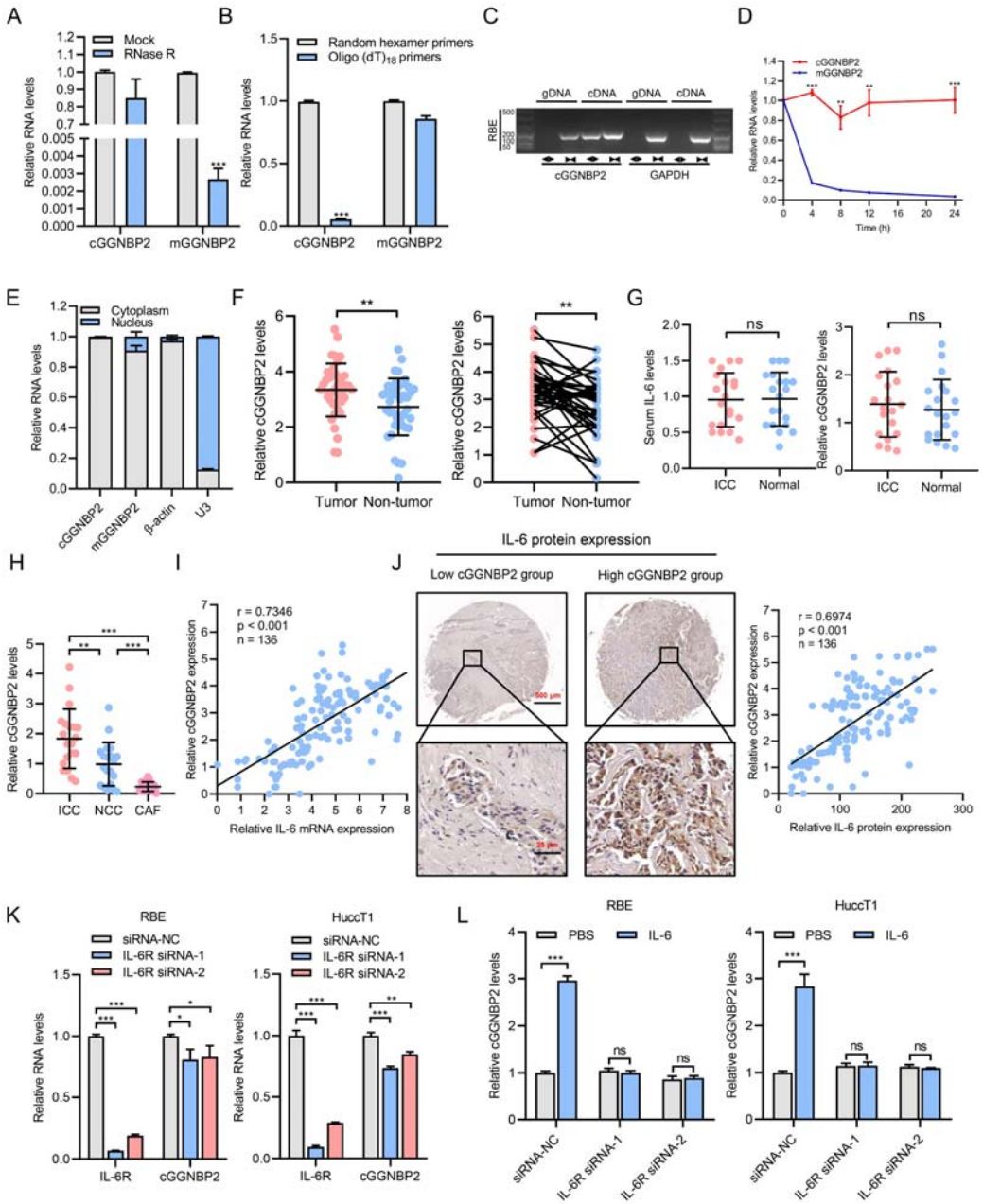

Fig. S3. Identification of cGGNBP2 and its subcellular localization. (A) qRT-PCR analyses for the relative expression of cGGNBP2 and GGNBP2 mRNA after treatment with RNase R in RBE cells. **(B)** Random hexamer or oligo $(dT)_{18}$ primers were used in the reverse transcription experiments. The relative RNA levels were evaluated by qRT-PCR. **(C)** qRT-PCR products with divergent primers showing the circularization of

cGGNBP2. GAPDH used as control. **(D)** The relative RNA levels of cGGNBP2 and mGGNBP2 were assessed by qRT-PCR after treatment with Actinomycin D at the indicated time points in RBE cells. **(E)** Cytoplasmic and nucleus fraction assay are showing that cGGNBP2 and mGGNBP2 localized in the cytoplasm of RBE cells. β-actin and U3 were used as positive controls in the cytoplasm and nucleus, respectively. **(F)** Relative cGGNBP2 expression in tumor tissues and matched non-tumor tissues of 136 ICC patients. **(G)** Left, serum IL-6 levels of 20 ICC patients and 20 patients with hepatic hemangioma were comparable. Right, relative cGGNBP2 expression in ICC and normal hepatic hemangioma tissues. **(H)** ICC cells, non-cancerous cholangiocytes and CAFs were isolated from fresh tumor and non-tumor tissues of 20 ICC patients. The relative cGGNBP2 levels were assessed by qRT-PCR in these three cell types. **(I)** The correlation between the relative cGGNBP2 expression and relative IL-6 mRNA expression of 136 tumor tissues. **(J)** Left, representative IHC staining images of IL-6 expression with relatively low or high expression in ICC tissues. Right, the correlation between the IHC staining scores of IL-6 and cGGNBP2 expression in 136 tumor tissues. **(K)** Relative expression of IL-6R and cGGNBP2 in the indicated cells. **(L)** Relative expression of cGGNBP2 by qRT-PCR assays in the indicated cells, with or without treatment with IL-6. cDNA, complementary DNA; gDNA, genomic DNA. ns, not significant; *, $P < 0.05$; **, $P < 0.01$; ***, $P < 0.001$.

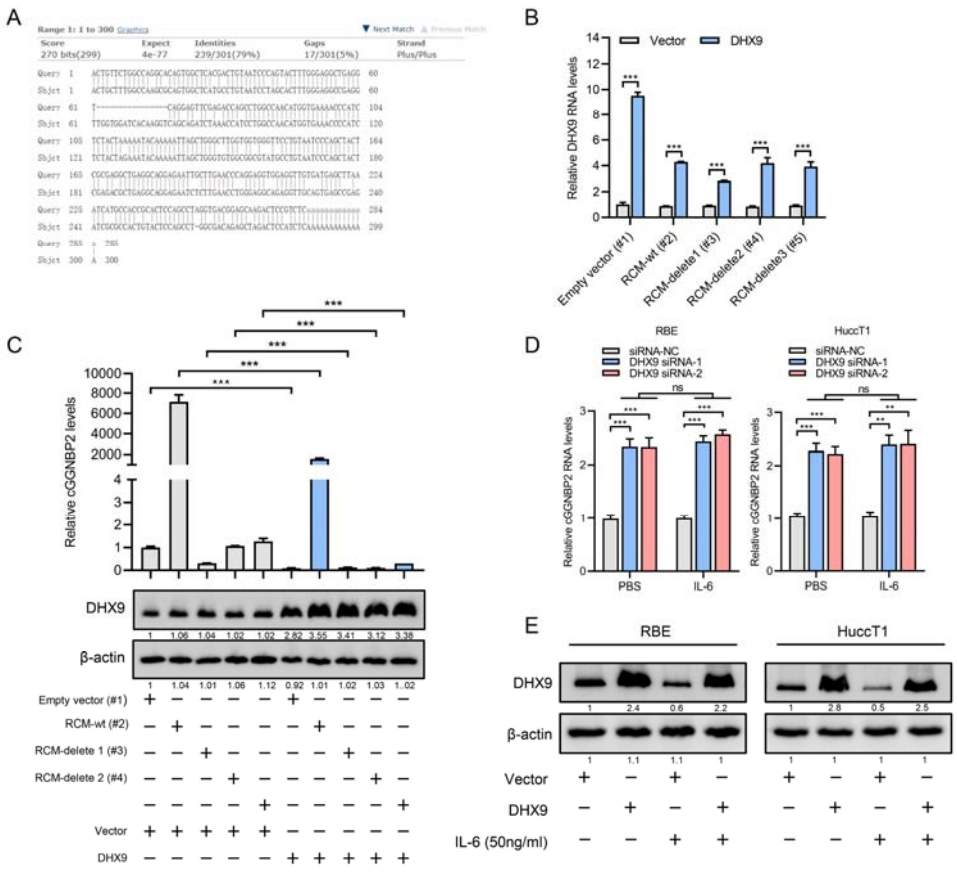

Fig. S4. DHX9 regulates the expression of cGGNBP2. (A) The sequence of intron 2 (chr17: 36545818-36554819) was aligned to that of intron 6 (chr17: 36567777-36577982) of the GGNBP2 gene by using BLAST (https://blast.ncbi.nlm.nih.gov/Blast.cgi). Highly reverse complementary sequences (79% identity over 301 nucleotides) were found and termed as FRCM (reverse complementary match in intron 2) and RRCM (reverse complementary match in intron 6), respectively. **(B)** Relative DHX9 mRNA expression in the indicated cells. **(C)** (top) qRT-PCR assays showed the relative expression of cGGNBP2 in the indicated RBE cells; (bottom) WB assays showed successful overexpression of DHX9 expression levels. **(D)** Relative cGGNBP2 expression in DHX9-depletion cells treated with IL-6 or PBS. **(E)** WB assays showed the relative DHX9 protein expression levels in the indicated cells. **, $P < 0.01$; ***, $P < 0.001$; ns, not significant.

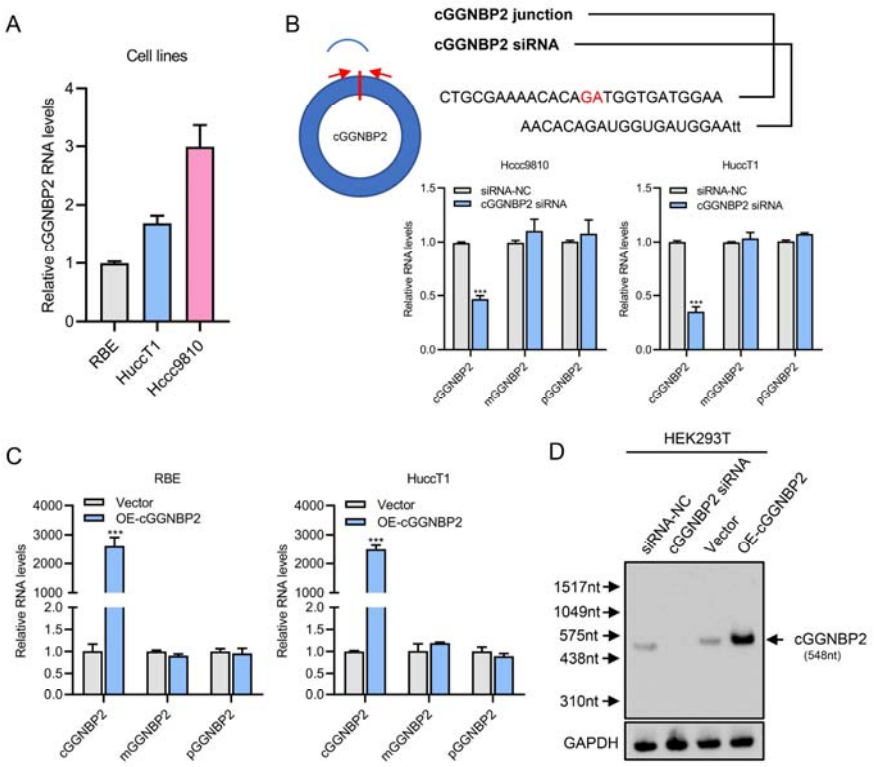

Fig. S5. Relative expression of cGGNBP2 in ICC cell lines. (A) qRT-PCR assays showed relative cGGNBP2 expression in three ICC cell lines. **(B)** Construction of junction-specific siRNA (top) and qRT-PCR assays showed relative RNA expression in RBE and HuccT1 cells (bottom). **(C)** Relative RNA expression levels after transfection of indicated vectors. **(D)** NB assays showed 548 nt cGGNBP2 in HEK293T cells using junction probe. NB, northern blot. ***, $P < 0.001$.

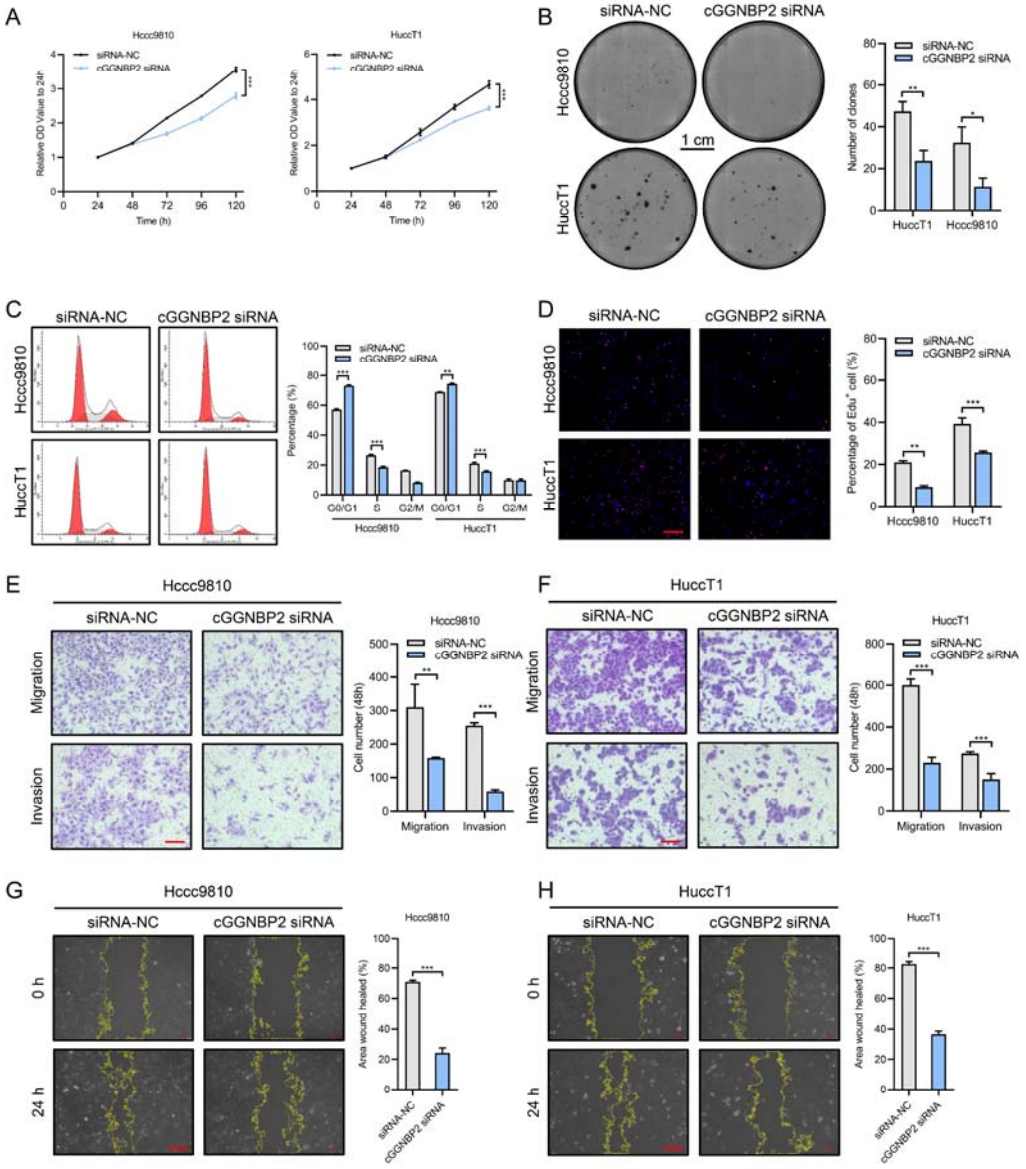

Fig. S6. Knockdown of cGGNBP2 inhibits ICC cells cell growth and metastasis in vitro. (A) CCK8 assays and **(B)** colony formation assays showed cGGNBP2 depletion inhibited cell growth of Hccc9810 and HuccT1 cells. **(C)** Cell cycle assays showed knockdown of cGGNBP2 increased the G0/G1 fraction and decreased the S fraction in Hccc9810 and HuccT1 cells. **(D)** EdU assays showed the capacity of DNA duplication in cells transfected with siRNA-NC and junction-specific cGGNBP2-siRNA. Scale bar,

100 μm. **(E)** and **(F)** The migration and invasion capacity were determined in indicated ICC cells. Scale bar, 100 μm. **(G)** and **(H)** Wound healing assays showed the migration capacity of indicated ICC cells. Scale bar, 100 μm. ICC, intrahepatic cholangiocarcinoma; CCK8, cell counting kit 8. *, $P < 0.05$; **, $P < 0.01$; ***, $P < 0.001$.

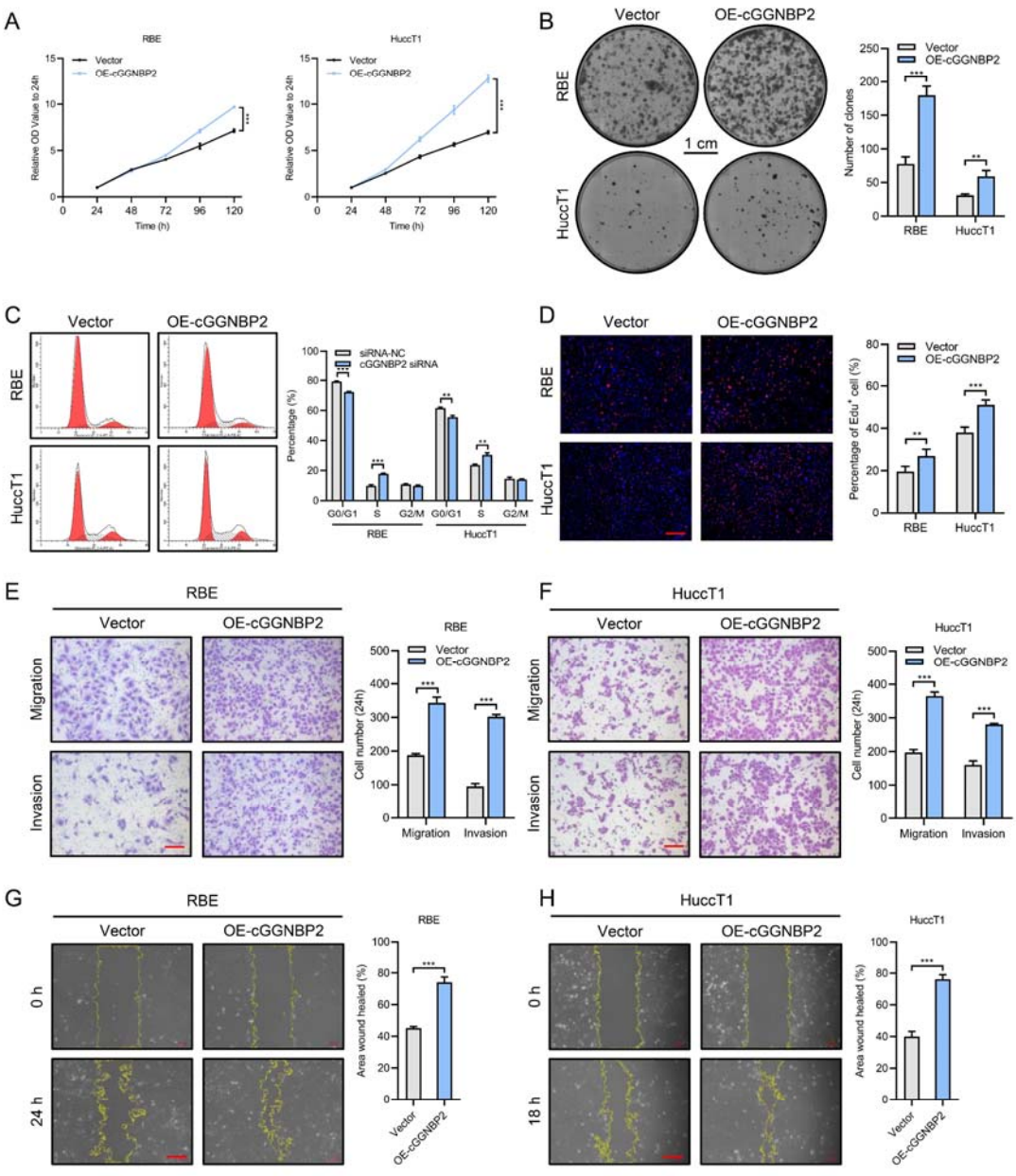

Fig. S7. Overexpression of cGGNBP2 promotes ICC cells cell growth and metastasis in vitro. (A) CCK8 assays and **(B)** colony formation assays showed cGGNBP2 overexpression facilitated cell growth of RBE and HuccT1 cells. **(C)** Cell cycle assays showed enhanced cGGNBP2 expression decreased the G0/G1 fraction and increased the S fraction in RBE and HuccT1 cells. **(D)** EdU assays showed the capacity

of DNA duplication in cells transfected with vector and OE-cGGNBP2 plasmid. Scale bar, 100 μm. **(E)** and **(F)** The migration and invasion capacity were determined in indicated ICC cells. Scale bar, 100 μm. **(G)** and **(H)** Wound healing assays showed the migration capacity of indicated ICC cells. Scale bar, 100 μm. *, $P < 0.05$; **, $P < 0.01$; ***, $P < 0.001$.

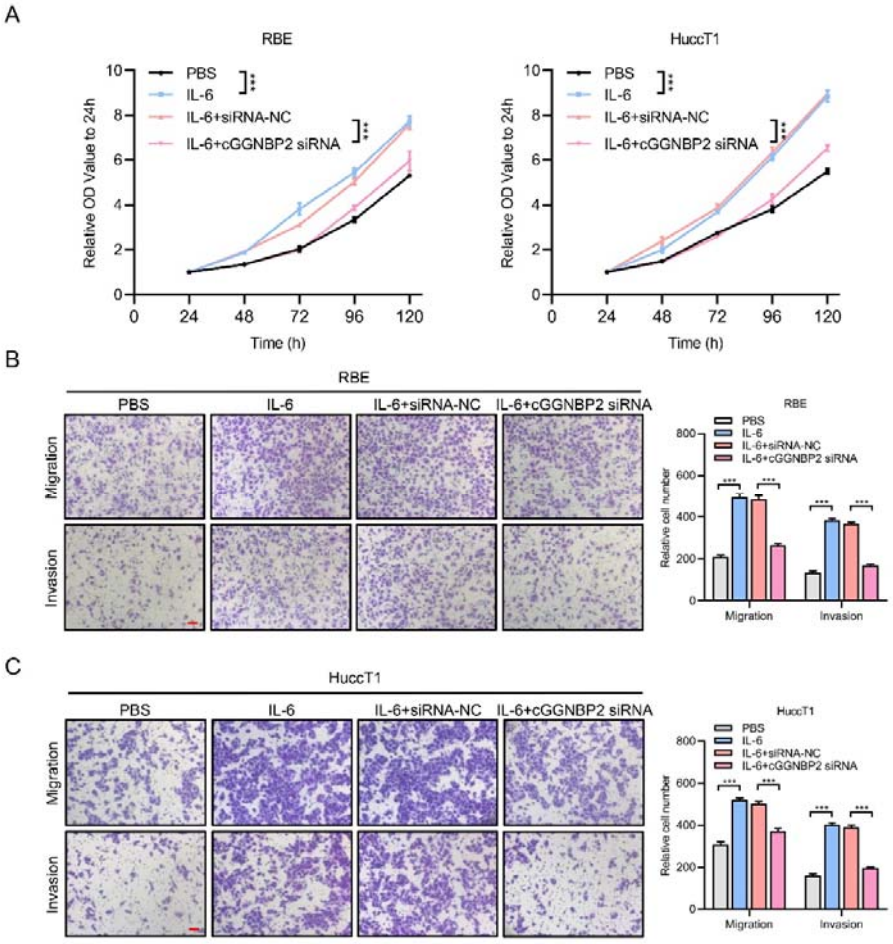

Fig. S8. cGGNBP2 depletion abolishes most of the effect of IL-6 on promoting ICC cell growth and metastasis. (A) CCK8 assays showed cell growth of RBE and HuccT1 cells. **(B)** and **(C)** The migration and invasion capacity were determined in indicated ICC cells. Scale bar, 100 μm. ***, $P < 0.001$.

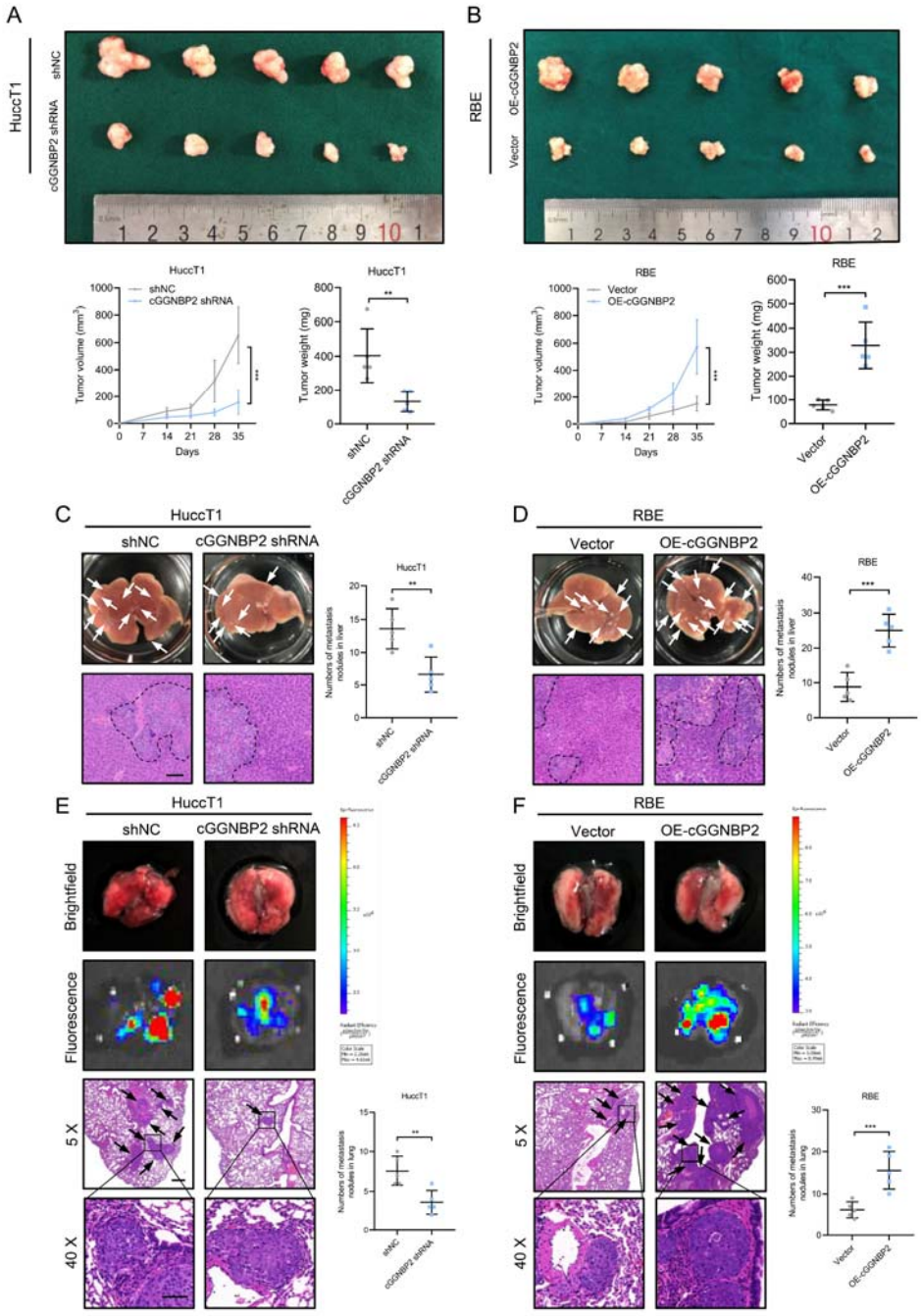

Fig. S9. cGGNBP2 promotes tumor growth and metastasis in vivo. (A) and **(B)** Tumor volume and weight of subcutaneous xenografts in nude mice implanted with indicated HuccT1 and RBE cells. **(C)** and **(D)** Decreased (C) and increased (D) tumor metastatic foci formed in the livers of nude mice implanted with cGGNBP2-

knockdown HuccT1 cells and cGGNBP2-ovexpression RBE cells. Left, top, representative images indicated the livers with metastatic foci (arrows). Left, bottom, representative HE staining of metastatic lesions (dotted line) in the livers. scale bar, 100 μm. Right, the number of metastatic foci formed in the livers for each group. **(E)** and **(F)** Tumor metastatic foci formed in the lungs of nude mice through vein tail injection with cGGNBP2-knockdown HuccT1 cells or cGGNBP2-ovexpression RBE cells. Top, representative lungs and relative fluorescence images for each group. Bottom, left, representative HE staining of metastatic lesions (arrows) in the lungs; scale bars, 100 μm (upper), 25 μm (lower). Bottom, right, the number of metastatic foci formed in the lungs for each group; dot plot reflected data points from independent experiment. (n=5 for each group). **, $P < 0.01$; ***, $P < 0.001$.

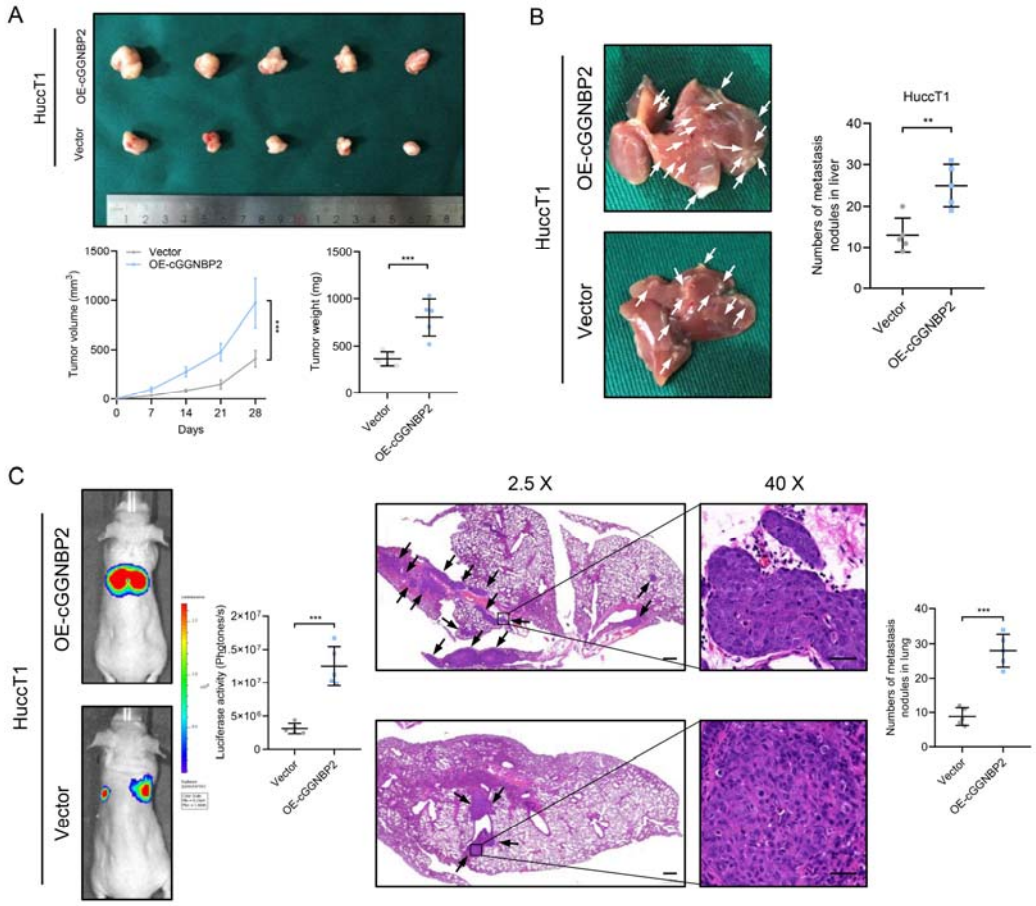

Fig. S10. cGGNBP2 promotes tumor growth and metastasis in vivo. (A) Tumor volume and weight of subcutaneous xenografts in nude mice implanted with cGGNBP2-overexpressed HuccT1 or control cells. **(B)** Left, representative images indicated the livers with metastatic foci (arrows). Right, Statistical analysis of the number of metastatic foci formed in the livers for each group. **(C)** Left, representative bioluminescent images of lungs after injection of indicated HuccT1 cells via tail vein. Right, representative HE staining of metastatic lesions (black arrows) in the lungs and relative statistical analysis. Scale bars, 100 μm (left), 25 μm (right). n=5 for each group. **, $P < 0.01$; ***, $P < 0.001$.

A

Transcript id	Exon information			
NM_024835	Spliced_len	Exon Number	Exon Sizes	Exon Offsets
	548	4	81, 254, 99, 114	0, 2262, 5952, 12841
Protein coding potential				
IRES Elements	Parameter Index			
	Position (start–end)		R Score	With Pseudoknot (Y/N)
	57–195		1.614802	Y
	40–185		1.363636	N
Open Reading Frame (ORF)	Start Position		End Position	Protein Length
	1		1>>7	184 aa
	MVMEFPDNVL NLDGHQNWGA QLKQFIQRHG MLKQQDLSIA MVVTSREVLS ALSQLVPCVG CRRSVERLFS QLVESGNPAL EPLTVGPKGV LSVTRSCMTD AKKLYTLFYV HGSKLNDMID AIPKSKKNKR CQLHSLDTHK PKPLGGCKMD VWELMSQECR DFVVLTDSSC LLETLETYLR KHRV*			
	Note: (1). nr represents n rounds(n<3); (2). * represents a stop codon.			

B

IRES-WT

57-126:

TGCACAGCTAAAGCAGTTCATTCAGCGACATGGTATGCTTAAGCAACAGGATCTAAGTATTGCCATGGTG

127-195:

GTGACATCACGCGAAGTCCTGAGTGCACTTTCTCAGCTTGTCCCATGTGTTGGTTGTCGTCGCAGTGTG

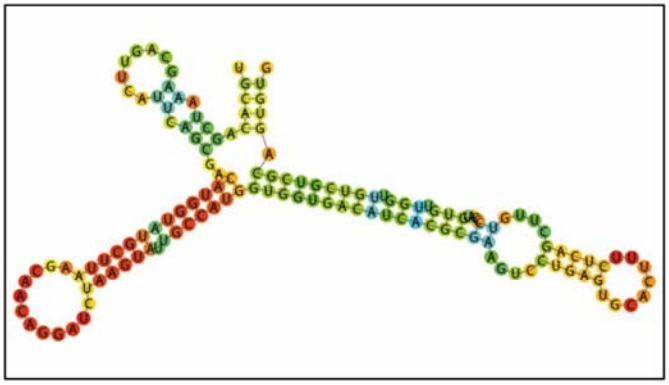

C

IRES-MUT

57-126:

TGCACAGCTAAAGCAGTTCATTCAGCGACATGGTATGCTTAAGTAACATTACTTTAGTATTGCCATGGTG

127-195:

GTGACATCACGCGAAGTCCTGAGTGCATGCACTCAGCACTTCATATGCGCTGGATGTCGTCGCAGTGTG

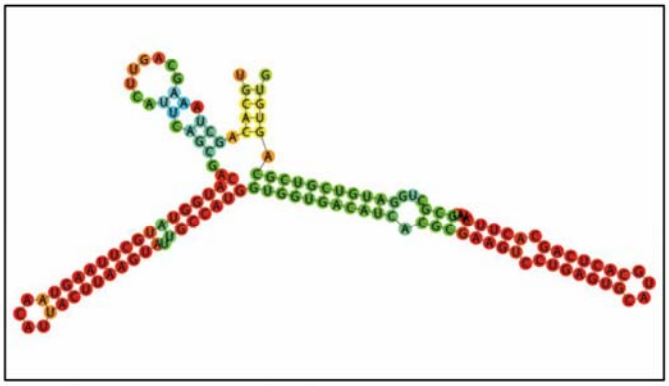

Fig. S11. Predicted IRES site and secondary structure. (A) The IRES site was predicted using circRNADb(11) (http://reprod.njmu.edu.cn/cgi-bin/circrnadb/circRNADb.php). **(B)** Sequences and predicted secondary structure of

IRES. **(C)** The mutation sites within the IRES in cGGNBP2 and its predicted secondary structure (marked in red). IRES, internal ribosomal entry site.

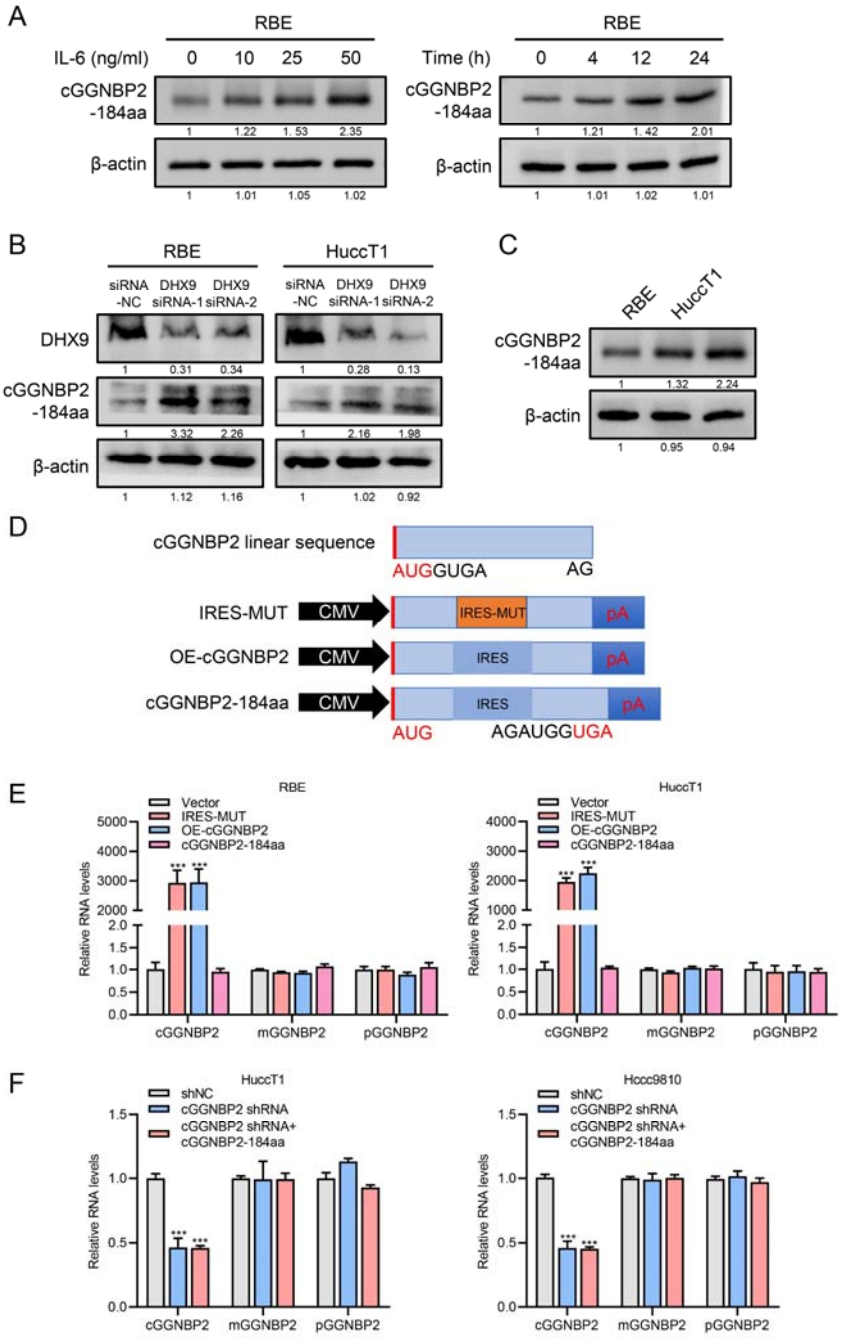

Fig. S12. IL-6 regulates the expression of cGGNBP2-184aa in ICC cells. (A) The relative cGGNBP2-184aa expression in RBE cells treated with IL-6 at the indicated concentration or time point. **(B)** WB assays showed DHX9 depletion increased the

expression level of cGGNBP2-184aa in ICC cells. **(C)** The relative cGGNBP2-184aa expression in ICC cell lines. **(D)** Vectors were constructed according to the linear sequences of cGGNBP2. cGGNBP2-184aa plasmid was constructed by cloning cGGNBP2-184aa ORF into vector. **(E)** qRT-PCR assays showed the relative RNA levels in cells transfected with indicated vectors. ***, $P < 0.001$ versus vectors. **(F)** qRT-PCR assays showed the relative RNA levels in indicated cells. ***, $P < 0.001$ versus shNC. mGGNBP2, mRNA of GGNBP2; pGGNBP2, pre-mRNA of GGNBP2.

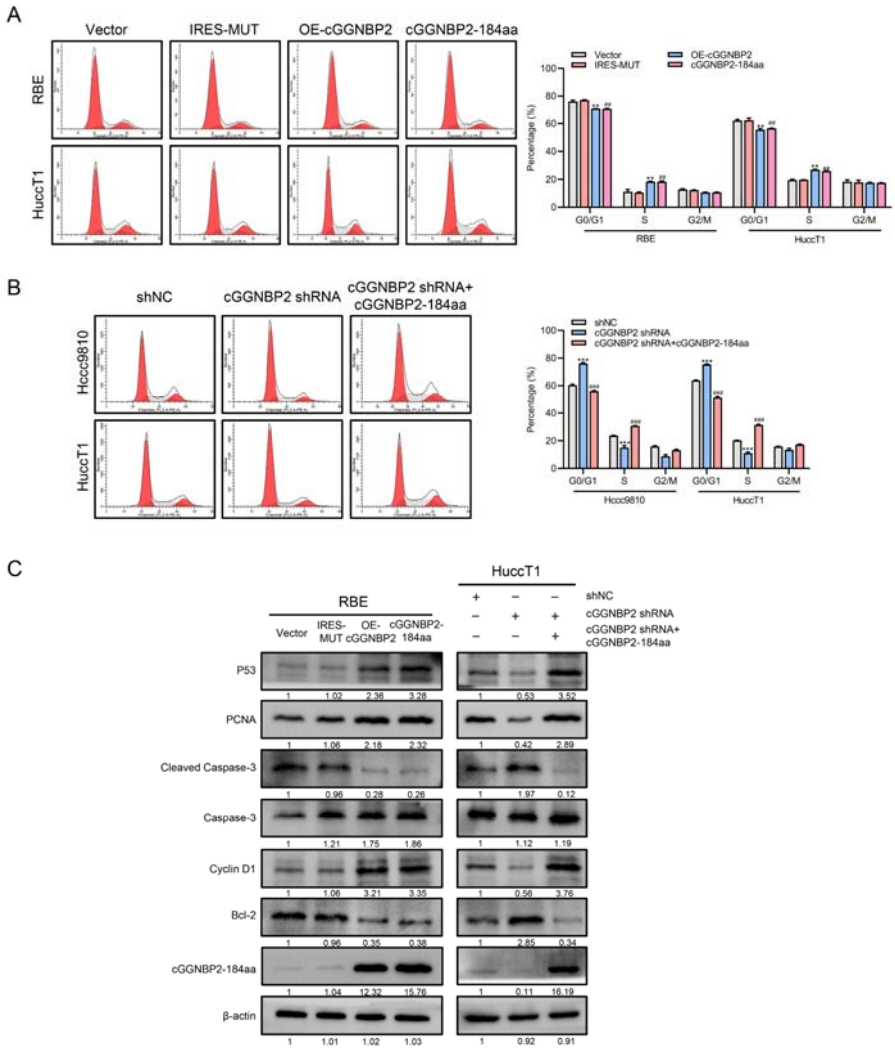

Fig. S13. cGGNBP2-184aa promotes cell cycle and inhibits apoptotic program that contribute to tumor cell growth. (A) Cell cycle assays showed cGGNBP2-184aa overexpression decreased the G0/G1 fraction and increased the S fraction in RBE and HuccT1 cells. **, $P < 0.01$ versus IRES-MUT. $^{\#\#}$, $P < 0.01$ versus vector. **(B)** Overexpression of cGGNBP2-184aa ORF rescued the inhibited effect of cGGNBP2 knockdown on cell cycle process. ***, $P < 0.001$; $^{\#\#\#}$, $P < 0.001$ versus shNC. **(C)** WB assays showed the expression of P53, PCNA, Cyclin D1 (contributing to cell growth) and Cleaved Caspase-3, Bcl-2 (contributing to apoptosis) in cells with regulation of cGGNBP2-184aa expression.

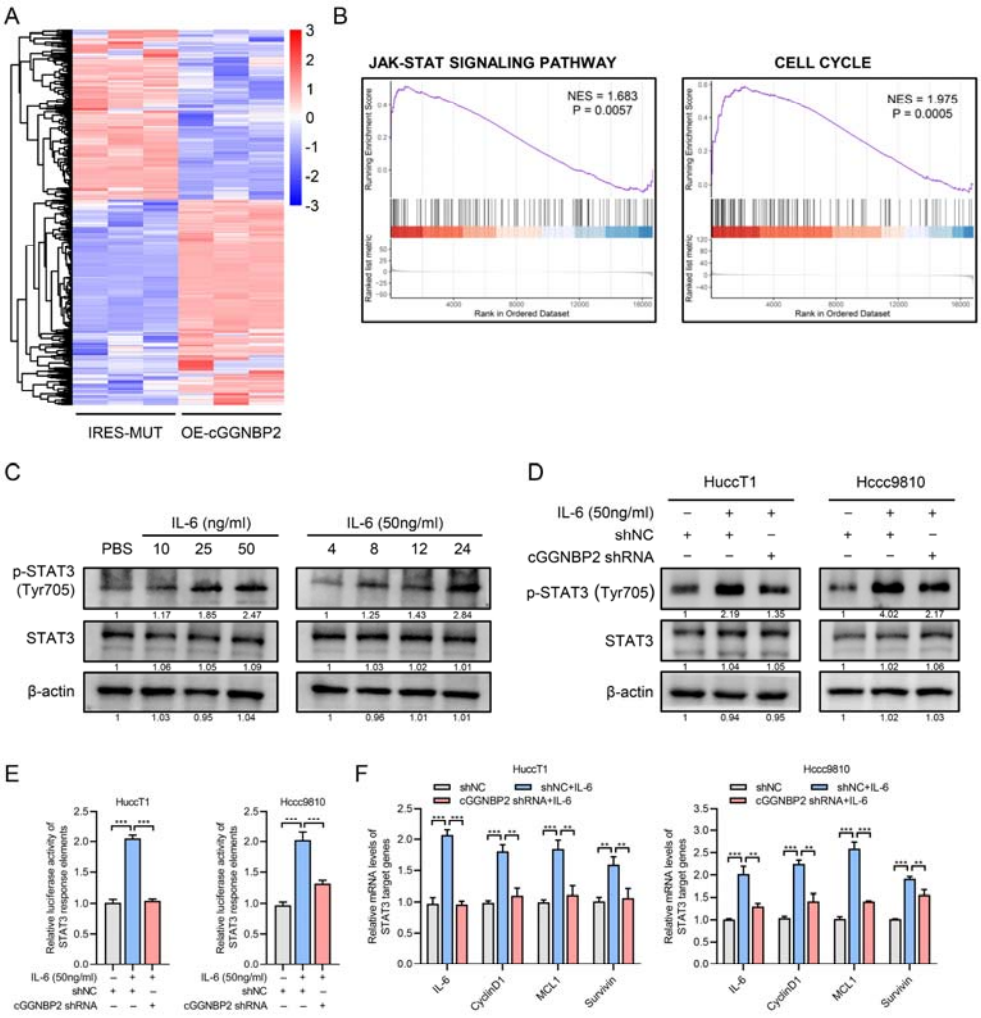

Fig. S14. cGGNBP2-184aa activates JAK-STAT signaling. (A) Heatmap of differentially expressed genes in upon cGGNBP2-184aa overexpression in RBE cells. The upregulated and downregulated genes were shaded with red and blue, respectively. **(B)** Gene expression levels of the subsets of genes involved in the JAK–STAT signaling pathway and cell cycle process. **(C)** WB assays showed the expression level of phosphorylated $STAT3^{Tyr705}$ and total STAT3 in cells treated with IL-6 at various concentration and time. **(D)** WB assays showed phosphorylated $STAT3^{Tyr705}$ and total STAT3 in the indicated cells. **(E)** Luciferase assays were performed to determine the

activity of STAT3 response elements in the indicated cells after treatment with IL-6. **(F)** qRT-PCR analysis for the relative mRNA expression of STAT3 target genes in the indicated cells after treatment with IL-6. **, $P < 0.01$; ***, $P < 0.001$.

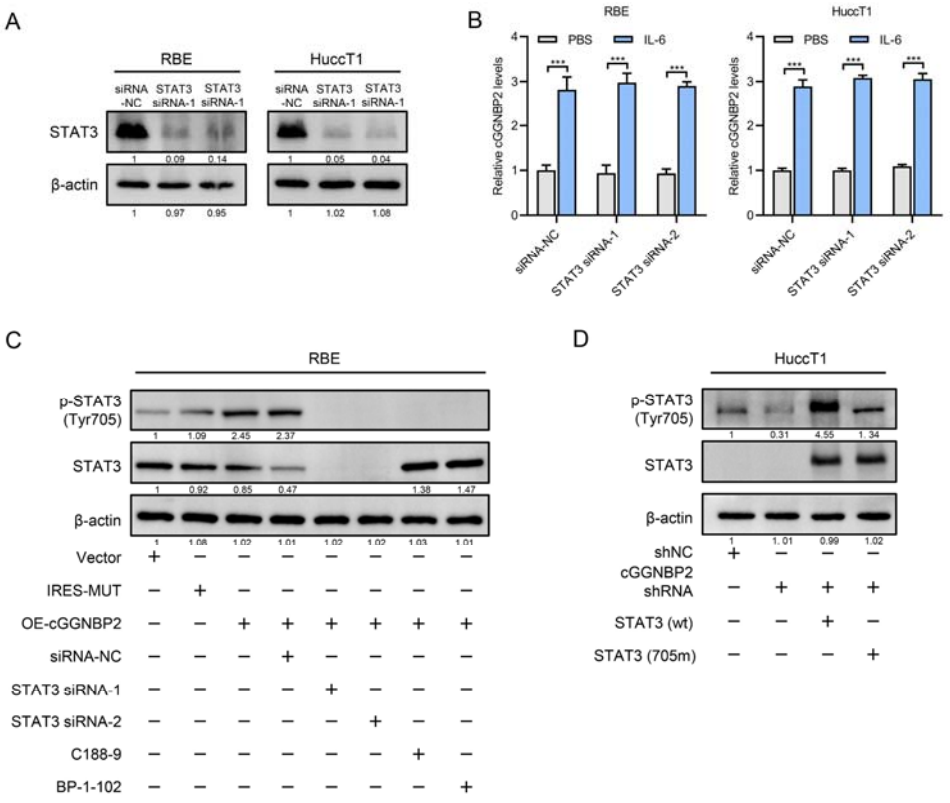

Fig. S15. cGGNBP2-184aa promotes the phosphorylation of STAT3 at Tyr705 site. **(A)** WB assays showed expression levels of STAT3 in ICC cells transfected with STAT3 siRNAs or the mock control. **(B)** qRT-PCR analysis showed relative expression of cGGNBP2 in the indicated ICC cells treated with IL-6 (50 ng/ml, 24 hours) or control PBS. **(C)** WB assays showed the phosphorylation levels of $STAT3^{Tyr705}$ in the indicated cells. cells were treated with C188-9 (20μM) and BP-1-102 (20μM) for 24 hours. **(D)** WB assays showed the phosphorylation status of STAT3 (Tyr705) in the indicated cells transfected with wild-type or Tyr705-mutated STAT3 plasmid. STAT3 was mutated as previously described[12], phenylalanine was introduced to substitute tyrosine, resulting in the incapacity of phosphorylation. ***, $P < 0.001$.

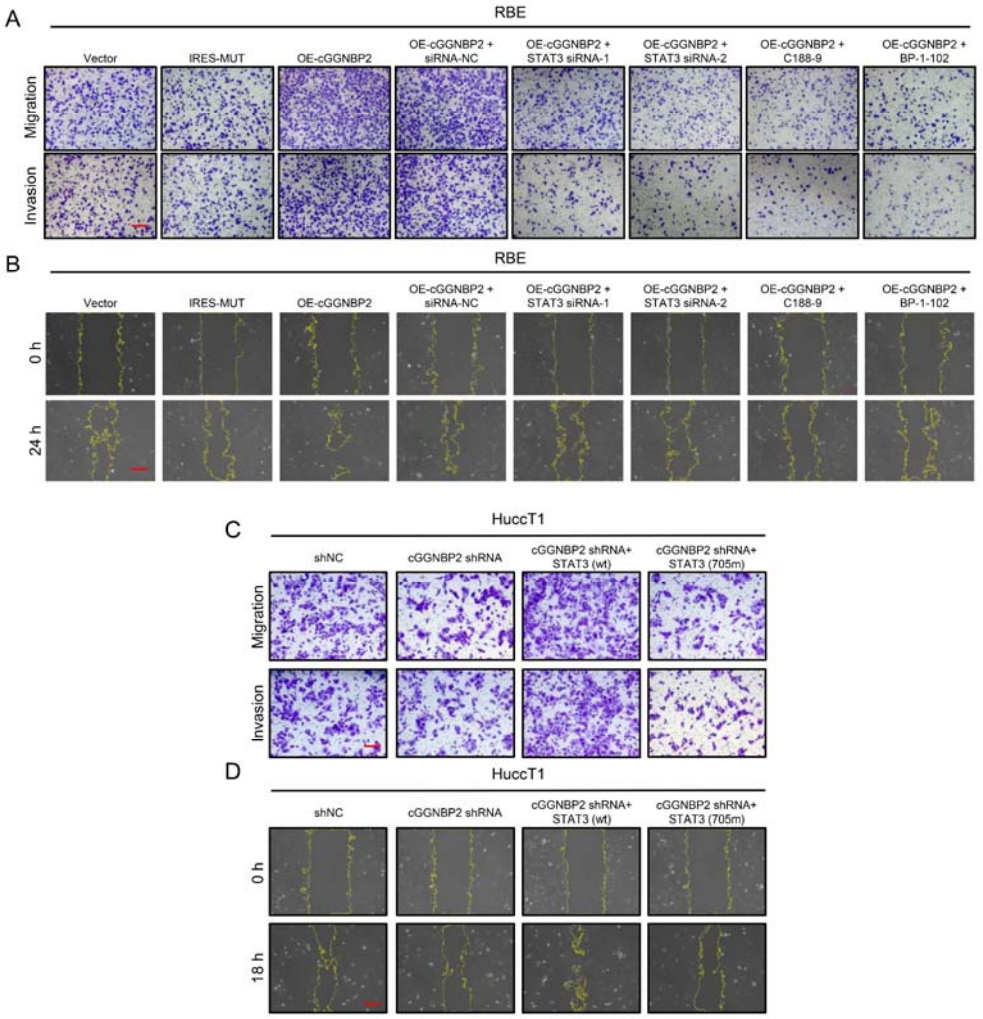

Fig. S16. Phosphorylated STAT3^{Tyr705} regulates ICC cell phenotypes. (A) Representative images of migration and invasion assays for indicated RBE cells transfected with STAT3 siRNA or treated with inhibitors. **(B)** Representative images of wound healing assays for indicated RBE cells transfected with STAT3 siRNA or treated with inhibitors. **(C)** Representative images of transwell migration and invasion assays for HuccT1 cells transfected with wild-type STAT3 or STAT3 (Tyr705 mutant). **(D)** Representative images of wound healing assays for HuccT1 cells transfected with wild-type or Tyr705-mutated STAT3 plasmid. Scale bar, 100 μm.

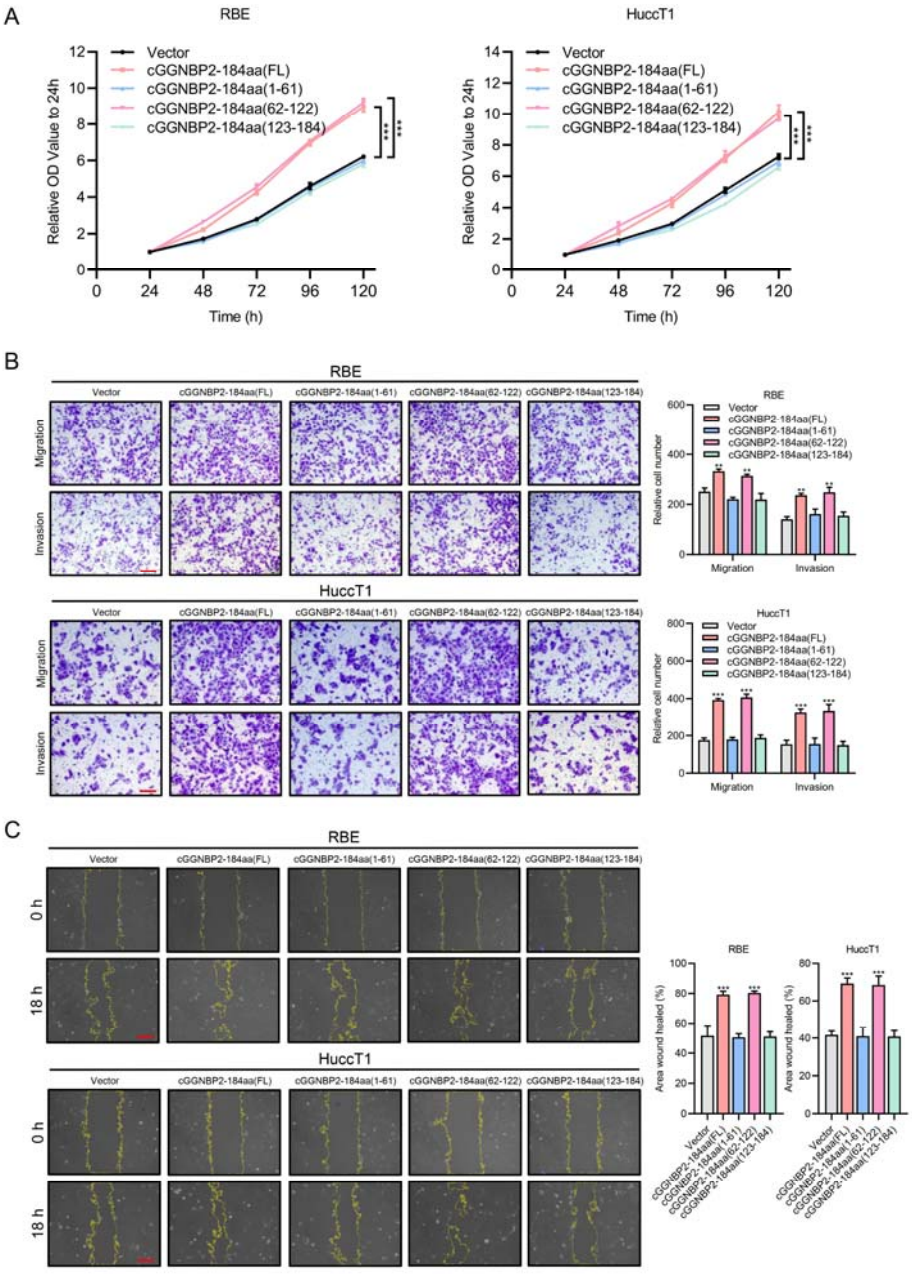

Fig. S17. The interaction region of cGGNBP2-184aa promotes cell proliferation, migration, and invasion in vitro. (A) CCK-8 assays showed cell proliferation of cells transfected with full-length or truncated cGGNBP2-184aa. **(B)** Left, representative images of transwell migration and invasion assays for ICC cells transfected with indicated plasmids expressing full-length and deletion mutants. Right, the relative

statistical analyses. **(C)** Left, representative images of wound healing assays for ICC cells transfected with indicated plasmids expressing full-length and deletion mutants. Right, the relative statistical analyses. **, $P < 0.01$; ***, $P < 0.001$ versus vector.

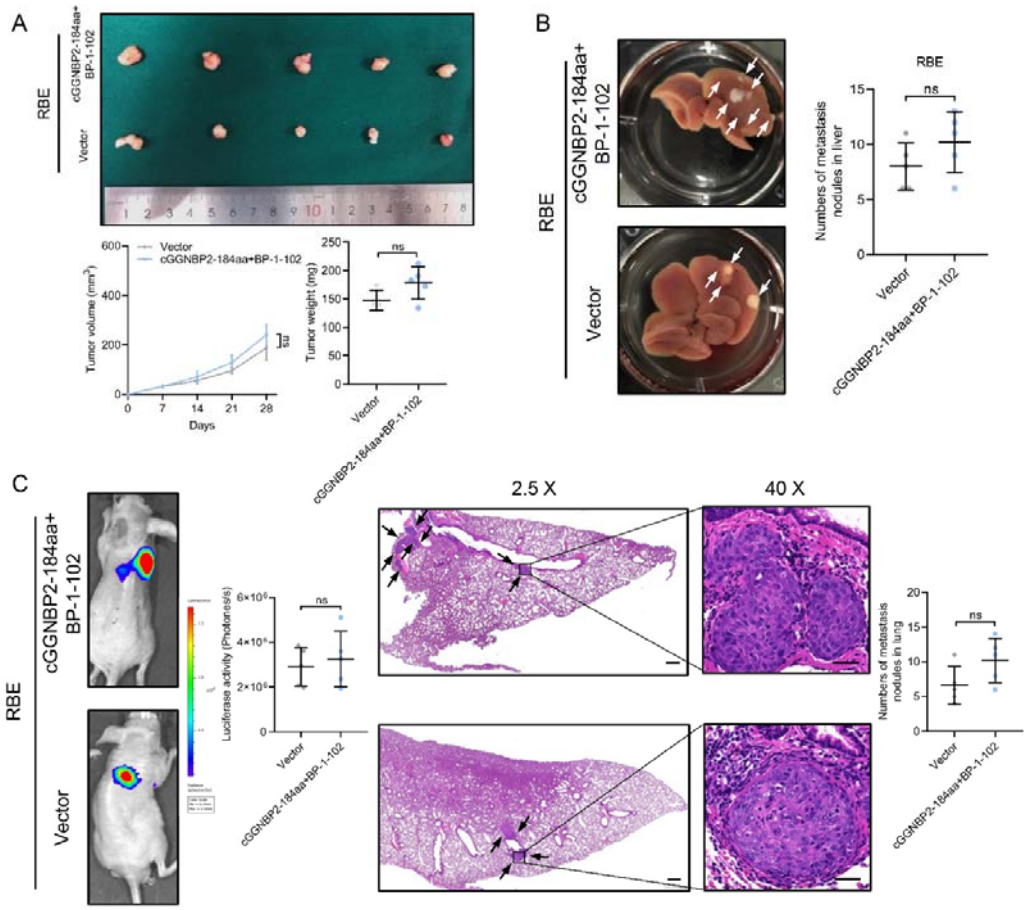

Fig. S18. STAT3 inhibitor abolishes abolish vast majority of the effect of cGGNBP2-184aa on promoting ICC cell growth and metastasis in vivo. (A) Tumor volume and weight of subcutaneous xenografts. **(B)** Left, representative images indicated the livers with metastatic foci (arrows). Right, Statistical analysis of the number of metastatic foci formed in the livers for each group. **(C)** Left, representative bioluminescent images of lungs. Right, representative HE staining of metastatic lesions (black arrows) in the lungs and relative statistical analysis. Scale bars, 100 μm (left), 25 μm (right). BP-1-102 (STAT3 inhibitor) or PBS was administered through oral gavage (3 mg/kg body weight) every day after establishment of in vivo models using cGGNBP2-184aa overexpressed RBE cells until sacrifice. n=5 for each group. ns, not significant.

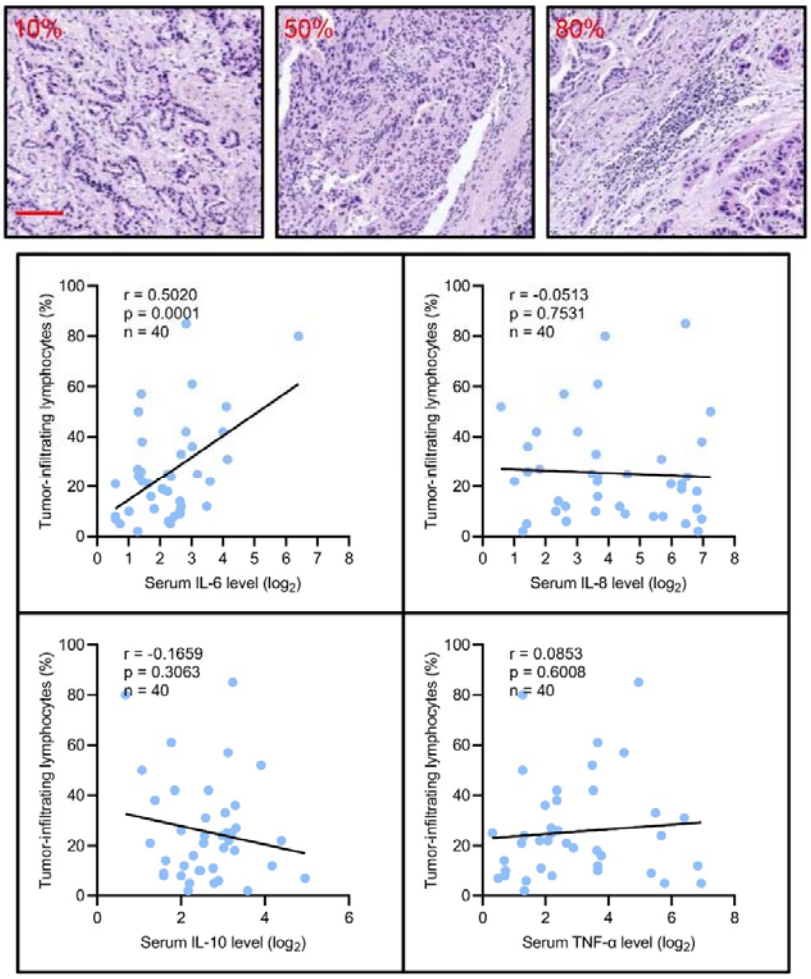

Fig. S19. IL-6 promotes tumor infiltrating lymphocytes in ICC. Top, representative images showed tumor infiltrating lymphocytes in ICC tissues**. Bottom**, correlation analyses between TILs and serum cytokines in 40 ICC patients. Only serum IL-6 levels positively correlated to TILs. TIL, tumor infiltrating lymphocyte. Scale bar, 25 μm.

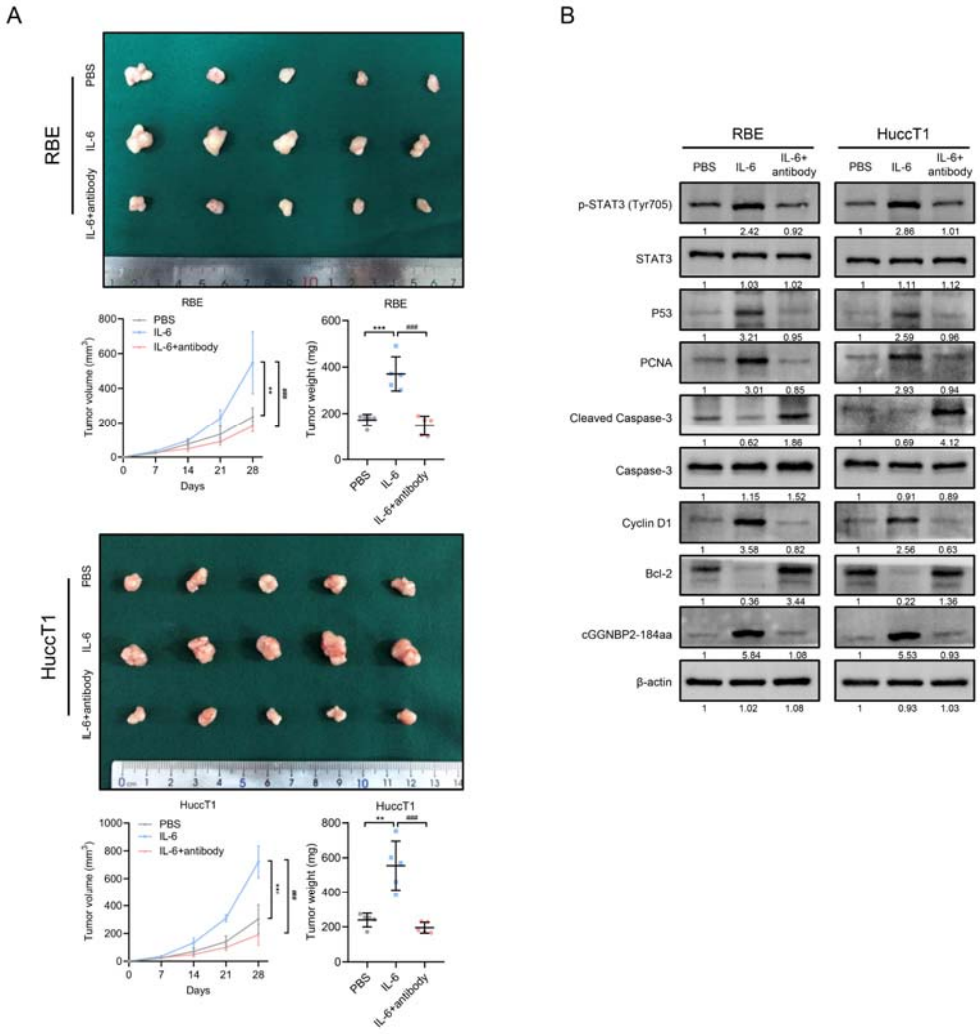

Fig. S20. In vivo assays confirm the role of IL-6/cGGNBP2 axis. (A) Representative images of subcutaneous xenografts. RBE or HuccT1 cells were subcutaneously injected to establish models. Then the mice were intraperitoneally injected with PBS or recombinant human IL-6 (2 mg/kg body weight, three times a week). IL-6 neutralizing antibody (Proteintech, 69001-1-Ig, 10 mg/kg body weight) or saline solution were intraperitoneally injected prior to administrating IL-6. **(B)** WB assays showed the expression of P53, PCNA, Cyclin D1 (contributing to cell growth) and Cleaved Caspase-3, Bcl-2 (contributing to apoptosis) in cells with regulation of cGGNBP2-184aa expression. **, $P < 0.01$; ***, $P < 0.001$.

Table S1. Baseline characteristics of 160 ICC patients according to serum IL-6 levels.

Variables	Low serum IL-6 (n=77)	High serum IL-6 (n=83)	P value
Age, year, >60/≤60	31/46	37/46	0.633
Gender, female/male	40/37	37/46	0.502
Hepatolithiasis, present/absent	14/63	16/67	0.859
CA19-9, >22/≤22	37/40	63/20	0.026
Tumor size, cm, >5/≤5	32/45	61/22	<0.001
Tumor number, multiple/solitary	18/59	35/48	0.039
Differentiation, poor/well-moderate	13/54	19/64	0.396
Microvascular invasion, present/absent	5/72	11/72	0.192
Lymph node, positive/negative	10/67	27/56	0.005
Cirrhosis, with/without	30/47	25/58	0.341
TNM stage, III/I- II	32/45	55/28	0.034

ICC, intrahepatic cholangiocarcinoma; IL-6, interleukin-6; TNM, tumor-node-metastasis; CI, confidence interval.

Table S2. Differentially expressed circRNAs.

circ_ID	Source gene	Gene name	IL-6 readcount (average)	Ctrl_readcount (average)	IL-6 TPM (average)	Ctrl TPM (average)	log2FoldChange (IL-6 vs Ctrl)	P-value (IL-6 vs Ctrl)	Chr	Start	End	Splice length
hsa_circ_0023891	ENSG00000073921	PICALM	8.438864706	1.019724886	251.8061393	31.13712791	1.2524	0.0051903	chr11	85974707	86031611	1814
hsa_circ_0019172	ENSG00000138190	EXOC6	8.328867076	1.011369499	247.543962	30.59226628	1.252	0.0052116	chr10	92893348	92920050	787
hsa_circ_0003930	ENSG00000278311	GGNBP2	8.994919484	1.386570523	268.2939877	42.20057691	1.2444	0.0055937	chr17	36554819	36567776	548
hsa_circ_0004662	ENSG00000285441	SOD2	7.538909025	0.712324191	225.3665238	21.80573273	1.226	0.0057704	chr6	159682473	159688242	462
hsa_circ_0008383	ENSG00000119408	NEK6	9.116326482	1.693971218	271.6374814	51.53197209	1.1406	0.01109	chr9	124301935	124327445	651
hsa_circ_0017041	ENSG00000054267	ARID4B	7.682960057	1.068486286	227.4337581	32.70859909	1.1397	0.010681	chr1	235152705	235155112	292
hsa_circ_0002085	ENSG00000001630	CYP51A1	7.379349933	1.011369499	218.7616349	30.59226628	1.1159	0.012307	chr7	92123119	92131872	894
hsa_circ_0013222	ENSG00000023909	GCLM	8.582381068	1.742732619	254.3688115	53.10344327	1.1144	0.013068	chr1	93894613	93897898	378
hsa_circ_00013	ENSG00000114 7	KLHL24	10.835656	3.1023658	321.95742	94.619613	1.0873	0.01273	chr3	18364347	18367248	1726

68	96		29		47	82				9	4	
hsa_circ_0003959	ENSG00000270898	GPR75-ASB3	1.526786652	7.561579651	44.91912174	230.5737776	-1.0271	0.022026	chr2	53714383	53716743	376
hsa_circ_0007788	ENSG00000153406	NMRAL1	2.142742925	9.230941683	63.821873 8	281.0370644	-1.0836	0.015564	chr16	4466152	4469465	489
hsa_circ_0005405	ENSG00000086102	NFX1	3.133085517	10.93559644	93.38840685	332.7296191	-1.087	0.013028	chr9	33351559	33352719	305
hsa_circ_0005019	ENSG00000131873	CHSY1	9.006328853	24.77714946	267.3753041	754.2326024	-1.1584	0.001397 3	chr15	101235081	101235577	496
hsa_circ_0004596	ENSG00000175582	RAB6A	4.033041198	14.11923124	119.8280224	429.9683516	-1.218	0.003548 9	chr11	73707419	73718890	312
hsa_circ_0016662	ENSG00000154380	ENAH	1.849472827	9.63308005	55.2219426	293.3297814	-1.232	0.005880 5	chr1	225554905	225567414	344
hsa_circ_0003541	ENSG00000149289	ZC3H12C	0.646441 69	10.69645305	19.614766	326.2410389	-1.728	0.000119 05	chr11	110136662	110159490	1127

Table S3. Prognostic factors for overall survival and recurrence-free survival by the univariate Cox proportional hazards regression model.

Variables	Overall survival			Recurrence-free survival		
	HR	**95% CI**	***P***	**HR**	**95% CI**	***P***
Age, year, >60/≤60	0.748	0.455-1.230	0.253	1.188	0.770-1.828	0.439
Gender, female/male	0.731	0.443-1.206	0.220	0.788	0.531-1.170	0.237
Hepatolithiasis, present/absent	1.121	0.506-2.485	0.778	0.815	0.407-1.633	0.564
CA19-9, >22/≤22	3.241	1.777-5.909	<0.001	2.060	1.350-3.145	0.001
Tumor size, cm, >5/≤5	2.240	1.309-3.832	0.003	1.869	1.245-2.806	0.003
Tumor number, multiple/solitary	2.433	1.486-3.985	<0.001	2.423	1.612-3.643	0.001
Differentiation, poor/well-moderate	2.070	1.229-3.485	0.006	1.436	0.921-2.237	0.110
Microvascular invasion, present/absent	3.440	1.847-6.407	<0.001	3.050	1.737-5.356	<0.001
Lymph node, positive/negative	2.192	1.281-3.753	0.004	1.79-	1.029-3.113	0.039
Cirrhosis, with/without	1.172	0.684-2.008	0.564	1.119	0.725-1.728	0.612
TNM stage, III/I- II	2.082	1.249-3.470	0.005	1.934	1.299-2.879	0.001
cGGNBP2 expression (high/low)	3.106	1.695-5.691	<0.001	2.175	1.410-3.353	<0.001

TNM, tumor-node-metastasis; HR, hazard ratio; CI, confidence interval; F, female; M, male.

Table S4. Independent prognostic factors for overall survival and recurrence-free survival by the multivariate Cox proportional hazards regression model.

Variables	Overall survival			Recurrence-free survival		
	HR	**95% CI**	***P***	**HR**	**95% CI**	***P***
CA19-9, >22/≤22	2.124	1.064-4.238	0.033	1.253	0.751-2.091	0.388
Tumor size, cm, >5/≤5	1.671	0.745-3.746	0.212	1.712	1.082-2.711	0.022
Tumor number, multiple/solitary	1.237	0.714-2.142	0.448	1.396	0.909-2.142	0.127
Differentiation, poor/well-moderate	3.244	1.841-5.715	0.001			
Microvascular invasion, present/absent	2.297	1.143-4.614	0.020	2.050	1.088-3.859	0.026
Lymph node, positive/negative	1.224	0.675-2.218	0.506	0.956	0.576-1.587	0.862
TNM stage, III/I- II	1.746	0.880-3.464	0.111	1.626	1.003-2.635	0.049
cGGNBP2 expression (high/low)	2.069	1.219-3.746	0.007	1.873	1.199-2.926	0.006

Potential confounders with P values less than 0.05 in univariate regression analyses were selected into multivariate regression models. TNM, tumor-node-metastasis; HR, hazard ratio; CI, confidence interval.

Table S5. RNA-Seq analyses of RNA-binding protein gene expression profiles affected by IL-6.

Gene name	Signal Intensity (FPKM)						Fold change	p value
	PBS-1	PBS-2	PBS-3	IL-6-1	IL-6-2	IL-6-3		
ADAR	28.38688	26.57305	25.67596	30.775259	38.21439	19.842255	1.101642204	0.660965758
DHX9	126.6981	114.1188	124.3208	91.546638	97.845306	96.276222	0.782357366	**0.003517197**
QKI	10.95921	1.925067	11.95702	1.528942	9.161062	9.553823	0.814926297	0.729002335
EIF4A3	74.79894	67.94447	75.94791	66.77887	71.221725	72.674957	0.963346679	0.432390007
EIF4G1	28.39552	27.77659	34.57	20.112015	26.114786	25.766102	0.793379256	0.098513566
FUS	1.657859	2.225609	1.291514	1.24891	1.183711	0.605829	0.587142139	0.104284662
HNRNPL	18.48278	19.02016	21.11193	14.349857	18.546068	15.112867	0.819054823	0.080531887
KHSRP	4.705699	5.666064	5.686309	4.285849	5.303301	3.516835	0.816161803	0.182123603
KHDRBS1	32.21642	33.48967	36.31725	32.28553	35.993256	34.880177	1.011131111	0.828326497
RBM20	0.36496	0.31559	0.509393	0.436522	0.386903	0.43383	0.142575412	0.728852267
MBNL1	0.246221	0.431625	0.435806	0.543412	0.970809	0.320109	0.193685183	0.297770508

Table S6. Primary antibodies used in this study.

Antigens	Antibody sources	Species	Dilution
DHX9	Abcam, ab183731	Rabbit monoclonal	1:1000 (WB)
			1:200 (IHC)
β-actin	Santa Cruz, sc-69879	Mouse monoclonal	1:1000 (WB)
GGNBP2	LSBio, LS-C166458	Rabbit polyclonal	1:1000 (WB)
cGGNBP2-184aa	Abclonal, customized	Rabbit polyclonal	1:500 (WB)
GAPDH	Absin, abs137959	Mouse monoclonal	1:2500 (WB)
Histone H3	Affinity, AF6359	Mouse monoclonal	1:2500 (WB)
STAT3	CST, 9139	Mouse monoclonal	1:1000 (WB)
			1:200 (IF)
p-STAT3 (Tyr705)	CST, 9145	Rabbit monoclonal	1:1000 (WB)
			1:200 (IHC)
p-STAT3 (Ser727)	CST, 94994	Rabbit monoclonal	1:1000 (WB)
HA	CST, 3724	Rabbit monoclonal	1:1000 (WB)
Flag	Millipore, F3165	Mouse monoclonal	1:1000 (WB)
Ki-67	Servicebio, GB13030-2	Rabbit monoclonal	1:500 (IHC)

Table S7. Primers used in this study.

Primer names	Sequences
cGGNBP2 forward	CGAAAACACAGATGGTGATGGA
cGGNBP2 reverse	TGATGTCACCACCATGGCAA
cKLHL24 forward	CGTGCAGCTATCCCAATTGC
cKLHL24 reverse	AATTTCCACACCTGACGGCT
cNEK6 forward	ACTCCCTAGTTCGTGCCCTC
cNEK6 reverse	CGAAAAGACAGCGTGTTGGG
cPICALM forward	CCCCTTTGGCCCTGTATCAG
cPICALM reverse	TTGAAGACCACCACCCAACT
cEXOC6 forward	CGTGATAGAATTCCAGAGGAAAGG
cEXOC6 reverse	GTGCGCATTTGGTTGGTCAT
cGCLM forward	TGCCACCAGATTTGACTGCA
cGCLM reverse	ATCCAGCTGTGCAACTCCAA
cCYP51A1 forward	TGACCAGAAAAGTCCTCCATACA
cCYP51A1 reverse	AAATGTCTTGCCTACCATGGT
cRBM34 forward	TGTTGGGAATTTGCCTGTTACA
cRBM34 reverse	GCGCTTTCCCAGAGAACGAA
cSOD2 forward	TGTGGGAGCACGCTTACTAC
cSOD2 reverse	GGCTGAAGAGCTATCTGGGC
mGGNBP2 forward	CAGGAGGGCGAAGAGAAAGG
mGGNBP2 reverse	AAGCATCTGCCATGTCTGCT
mGCLM forward	TGGAGTTGCACAGCTGGATT
mGCLM reverse	GTGCCCACTGATACAGCTGT
mRBM34 forward	GGAAGGGATGAGCAAACGGA
mRBM34 reverse	TCGCCGCGAAATAAGCTACT
mKLHL24 forward	TCACAGGGGTAGCTGCAATG
mKLHL24 reverse	AGTGTGGCTTCTTCGGTGAG
mNEK6 forward	ATAAGGGCAGGTGGTTCAGC
mNEK6 reverse	ATCACACGGTCTCCTGCAAG
mPICALM forward	TGCCTAGGATTTTGCCAGGG
mPICALM reverse	TGACATGCCAAGCACAAAGC
mCYP51A1 forward	ATGGAGGTTTCAGCCATGCA
mCYP51A1 reverse	TCTGCGTTTCTGGATTGCCT
mEXOC6 forward	AGAGTCACTACACCGGAGCT
mEXOC6 reverse	TGCTCCAGGTGTGTTGTGTT
mSOD2 forward	ACCAGCACTAGCAGCATGTT
mSOD2 reverse	TTGATGTGAGGTTCCAGGGC

pGGNBP2 forward	CTGCGCACTGGAGAAAGAGT
pGGNBP2 reverse	GACAGAGGTTACCGAGCCAC
Convergent cGGNBP2 forward	ATCACGCGAAGTCCTGAGTG
Convergent cGGNBP2 reverse	TCCCTTGGGCCCTACTGTTA
Divergent GAPDH forward	GGCCTCCAAGGAGTAAGA
Divergent GAPDH reverse	GCCCAATACGACCAAATCA
U6 forward	TCGGCAGCACATATACTAAAATTGG
U6 reverse	ACGAATTTGCGTGTCATCCT
U3 forward	TTCTCTGAGCGTGTAGAGCACCGA
U3 reverse	GATCATCAATGGCTGACGGCAGTT
β-actin forward	GGGAAATCGTGCGTGACATTAAG
β-actin reverse	TGTGTTGGCGTACAGGTCTTTG
DHX9 forward	TGCCTCCAAGAAAGTCCA
DHX9 reverse	TCCGCTTCCATTGTCGTAT
FRCM forward	GCTGAGGTCAGGAGTTCGAG
FRCM reverse	TGCGGTGGCATGATTTAAGC
RRCM forward	GAGATTCTCCTGCCTCAGCG
RRCM reverse	GGTGGATCACAAGGTCAGCA
EXON1 forward	GAGGAAACGACATTCGGAGC
EXON1 reverse	GGTTCCGACCTTCACCGTTT
IL-6R forward	TTGTTTGTGAGTGGGGTCCT
IL-6R reverse	TGGGACTCCTGGGAATACTG
IL-6 forward	AGAGGCACTGGCAGAAAACA
IL-6 reverse	GCTCTGGCTTGTTCCTCACT
Cyclin D1 forward	CTGATTGGACAGGCATGGGT
Cyclin D1 reverse	TCTTGCCACCTCCCTTCAAC
MCL1 forward	CATTCCTGATGCCACCTTCT
MCL1 reverse	TCGTAAGGACAAAACGGGAC
Survivin forward	GAACTGGCCCTTCTTGGAGG
Survivin reverse	CAGCCTTCCAGCTCCTTGAA

Table S8. Sequences of siRNA and shRNA used in this study.

Names	Sequences
cGGNBP2 siRNA sense	5’-AACACAGAUGGUGAUGGAATT-3’
cGGNBP2 siRNA anti-sense	5’-UUCCAUCACCAUCUGUGUUTT-3’
IL-6R siRNA-1 sense	5’-AGACUACGGUUUGAGCUCATT-3’
IL-6R siRNA-1 anti-sense	5’-UGAGCUCAAACCGUAGUCUGT-3’
IL-6R siRNA-2 sense	5’-CAACAUGGAUGGUCAAGGATT-3’
IL-6R siRNA-2 anti-sense	5’-UCCUUGACCAUCCAUGUUGTG-3’
DHX9 siRNA-1 sense	5’-CUGAUCACAACAGGAGCUUTT-3’
DHX9 siRNA-1 anti-sense	5’-AAGCUCCUGUUGUGAUCAGTT-3’
DHX9 siRNA-2 sense	5’-GGUUGAAGCUUACUCCGGATT-3’
DHX9 siRNA-2 anti-sense	5’-UCCGGAGUAAGCUUCAACCAC-3’
STAT3 siRNA-1 sense	5’-GCACCUUCCUGCUAAGAUUTT-3’
STAT3 siRNA-1 anti-sense	5’-AAUCUUAGCAGGAAGGUGCCT-3’
STAT3 siRNA-2 sense	5’-GGCUGGACAAUAUCAUUGATT-3’
STAT3 siRNA-2 anti-sense	5’-UCAAUGAUAUUGUCCAGCCAG-3’
siRNA-NC sense	5’-UUCUCCGAACGUGUCACGUTT-3’
siRNA-NC anti-sense	5’-ACGUGACACGUUCGGAGAATT-3’
FISH probe	
cGGNBP2	5’-cy3-ATTCCATCACCATCTGTGTTTTCGC-cy3-3’
AS	5’-cy3-TAAGGTAGTGGTAGACACAAAAGCG-cy3-3’
Northern probe	
cGGNBP2	5’- ATTTAACACATTATCAGGAAATTCCTCACCATCTGTG TTTTCGCAGATATGTTTCTAGTGTTTCTA-DIG-3’

References

1. Memczak S, Jens M, Elefsinioti A, Torti F, Krueger J, Rybak A, Maier L, et al. Circular RNAs are a large class of animal RNAs with regulatory potency. Nature 2013;495:333-338.

2. Yu J, Xu QG, Wang ZG, Yang Y, Zhang L, Ma JZ, Sun SH, et al. Circular RNA cSMARCA5 inhibits growth and metastasis in hepatocellular carcinoma. J Hepatol 2018;68:1214-1227.

3. Liu H, Lan T, Li H, Xu L, Chen X, Liao H, Chen X, et al. Circular RNA circDLC1 inhibits MMP1-mediated liver cancer via interaction with HuR. Theranostics 2021;11:1396-1411.

4. Olmeda D, Cerezo-Wallis D, Riveiro-Falkenbach E, Pennacchi PC, Contreras-Alcalde M, Ibarz N, Cifdaloz M, et al. Whole-body imaging of lymphovascular niches identifies pre-metastatic roles of midkine. Nature 2017;546:676-680.

5. Li H, Liu H, Fu H, Li J, Xu L, Wang G, Wu H. Peritumoral Tertiary Lymphoid Structures Correlate With Protective Immunity and Improved Prognosis in Patients With Hepatocellular Carcinoma. Front Immunol 2021;12:648812.

6. Yugawa K, Itoh S, Yoshizumi T, Iseda N, Tomiyama T, Toshima T, Harada N, et al. Prognostic impact of tumor microvessels in intrahepatic cholangiocarcinoma: association with tumor-infiltrating lymphocytes. Mod Pathol 2021;34:798-807.

7. Sha M, Jeong S, Qiu BJ, Tong Y, Xia L, Xu N, Zhang JJ, et al. Isolation of cancer-associated fibroblasts and its promotion to the progression of intrahepatic cholangiocarcinoma. Cancer Med 2018;7:4665-4677.

8. Pepe-Mooney BJ, Dill MT, Alemany A, Ordovas-Montanes J, Matsushita Y, Rao A, Sen A, et al. Single-Cell Analysis of the Liver Epithelium Reveals Dynamic Heterogeneity and an Essential Role for YAP in Homeostasis and Regeneration. Cell Stem Cell 2019;25:23-38.e28.

9. Li H, Lan T, Xu L, Liu H, Wang J, Li J, Chen X, et al. NCSTN promotes hepatocellular carcinoma cell growth and metastasis via β-catenin activation in a Notch1/AKT dependent manner. Journal of Experimental & Clinical Cancer Research 2020;39:128.

10. Consortium TU. UniProt: a worldwide hub of protein knowledge. Nucleic Acids Research 2018;47:D506-D515.

11. Chen X, Han P, Zhou T, Guo X, Song X, Li Y. circRNADb: A comprehensive database for human circular RNAs with protein-coding annotations. Sci Rep 2016;6:34985.

12. Tanaka T, Yamamoto Y, Muromoto R, Ikeda O, Sekine Y, Grusby MJ, Kaisho T, et al. PDLIM2 inhibits T helper 17 cell development and granulomatous inflammation through degradation of STAT3. Sci Signal 2011;4:ra85.